nature reviews physics

https://doi.org/10.1038/s42254-023-00659-z

Review article

Check for updates

Acoustic resonances in non-Hermitian open systems

Lujun Huang[1,8] ✉, Sibo Huang[2,8], Chen Shen[3,8], Simon Yves[4,8], Artem S. Pilipchuk[5,8], Xiang Ni[4], Seunghwi Kim[4], Yan Kei Chiang[6], David A. Powell[6], Jie Zhu[2], Ya Cheng[1], Yong Li[2] ✉, Almas F. Sadreev[5] ✉, Andrea Alù[4,7] ✉ & Andrey E. Miroshnichenko[6] ✉

Abstract

Acoustic resonances in open systems, which are usually associated with resonant modes characterized by complex eigenfrequencies, play a fundamental role in manipulating acoustic wave radiation and propagation. Notably, they are accompanied by considerable field enhancement, boosting interactions between waves and matter, and leading to various exciting applications. In the past two decades, acoustic metamaterials have enabled a high degree of control over tailoring acoustic resonances over a range of frequencies. Here, we provide an overview of recent advances in the area of acoustic resonances in non-Hermitian open systems, including Helmholtz resonators, metamaterials and metasurfaces, and discuss their applications in various acoustic devices, including sound absorbers, acoustic sources, vortex beam generation and imaging. We also discuss bound states in the continuum and their applications in boosting acoustic wave–matter interactions, active phononics and non-Hermitian acoustic resonances, including phononic topological insulators and the acoustic skin effect.

Sections

[1]The Extreme Optoelectromechanics Laboratory (XXL), School of Physics and Electronic Sciences, East China Normal University, Shanghai, China. [2]Institute of Acoustics, Tongji University, Shanghai, China. [3]Department of Mechanical Engineering, Rowan University, Glassboro, NJ, USA. [4]Photonics Initiative, Advanced Science Research Center, City University of New York, New York, NY, USA. [5]L. V. Kirensky Institute of Physics, Krasnoyarsk, Russia. [6]School of Engineering and Technology, University of New South Wales, Canberra, Australian Capital Territory, Australia. [7]Physics Program, Graduate Center, City University of New York, New York, NY, USA. [8]These authors contributed equally: Lujun Huang, Sibo Huang, Chen Shen, Simon Yves, Artem S. Pilipchuk. ✉e-mail: ljhuang@phy.ecnu.edu.cn; yongli@tongji.edu.cn; almas@tnp.krasn.ru; aalu@gc.cuny.edu; andrey.miroshnichenko@unsw.edu.au

Key points

- Acoustic resonances in open systems are associated with eigenmodes characterized by complex eigenfrequencies. These resonances arise in various acoustic systems whose features can be precisely engineered, making them promising for advanced sound manipulation with resonant metastructure devices.
- An emerging class of non-Hermitian resonances is that of acoustic bound states in the continuum, which are exotic resonances with a theoretically unbounded *Q*-factor, providing a versatile and powerful means of enhancing acoustic wave–matter interactions.
- By making use of the properties of active metamaterials and metasurfaces, acoustic resonances can be precisely engineered to feature active, nonlinear and non-reciprocal properties, as well as parity–time-symmetric wave phenomena, showing great potential for applications in enhanced acoustic wave control.
- Non-Hermitian Hamiltonians extend the common Hermitian dispersion to the complex plane, resulting in additional exotic features of the band structure. Among these, exceptional degeneracies and bandgaps with unconventional topologies yield exciting and unusually robust wave phenomena.

Introduction

Resonances are a universal phenomenon in nature, existing in open systems with a non-Hermitian Hamiltonian that involves interaction and energy exchange with the surrounding environment. Resonances usually involve enhanced amplitudes for a specific excitation frequency that matches an intrinsic frequency of the system. They occur in any wave system, including mechanical resonances, orbital resonances, Feshbach resonances, acoustic resonances, electromagnetic resonances and nuclear magnetic resonances. Acoustic resonances play a fundamental role in controlling the response of sound and governing acoustic wave–matter interactions. In that regard, they are at the core of developing acoustic devices for sound manipulation.

In the past two decades, the rise of acoustic metamaterials and metasurfaces has provided unprecedented freedom in tailoring acoustic resonances at any desired frequency[1,2]. These metastructures, namely artificial media obtained by arranging subwavelength structures in a periodic manner, largely rely on the local resonant properties of their constituents, called meta-atoms[3]. Each acoustic resonance in the reflection/transmission spectrum is correlated to an eigenmode of the non-Hermitian system[4]. These modes are characterized by complex eigenfrequencies[5–8], whose real and imaginary parts correspond to the resonance frequency and the half-linewidth of the resonance, respectively. Similar to their quantum-mechanical and electromagnetic counterparts, acoustic resonances play a crucial role in tailoring the effective properties of a metamaterial, such as bulk modulus or mass density[9–13]. As a landmark example, precisely engineered acoustic resonators have been used to realize negative bulk modulus[11], negative mass density[10,12], or double negativity (simultaneous negative bulk modulus and mass density)[13–18], which results in a negative index that is not available in natural materials.

Acoustic resonances also inherently enable efficient confinement of the pressure field, showing great potential for boosting acoustic wave–matter interactions. Among such resonant effects, acoustic bound states in the continuum[19,20] – exotic resonances with an infinite quality (*Q*) factor – have received tremendous attention in both fundamental physics and practical applications due to their extreme field confinement. The addition of active schemes to acoustic metastructures brings about many opportunities for creating highly reconfigurable and non-reciprocal devices whose properties go beyond what common passive resonances can offer. Furthermore, introducing balanced gain and loss into a coupled resonator results in parity–time (PT) symmetry phases and exceptional points (EPs)[21–23]. Besides this, acoustic resonances and metastructures have been a substantial part of the transposition of topological insulator concepts from electronics to classical waves in the past decade[24]. These systems thus make powerful tabletop platforms for investigating new topological phenomena driven by non-Hermiticity.

This Review aims to provide an overview of the fundamental physics of acoustic resonances in non-Hermitian open systems and their various applications (Fig. 1). We first review several types of acoustic resonance and discuss their applications in sound absorption, acoustic vortex generation, acoustic imaging and acoustic emission. We then survey the recent progress of acoustic BICs, which are unique acoustic resonances with infinite *Q*-factors. We discuss the features of active resonances and metamaterials, as well as their role in realizing non-reciprocity. We conclude with recent progress in non-Hermitian acoustics, including PT-symmetry and EPs as well as non-Hermitian topological acoustics, and provide our outlook on future perspectives.

Acoustic resonances in open systems

Resonances can be illustrated with a simple mass–spring model[3] (Fig. 2a). Consider a damped mass on a spring driven by an applied sinusoidal force. According to Newton's second law, we have

$$m\frac{\mathrm{d}^2x}{\mathrm{d}t^2} = F_0\sin(\omega t) - kx - c\frac{\mathrm{d}x}{\mathrm{d}t} \tag{1}$$

where m is the mass, x is the displacement of the mass from the equilibrium point, F_0 is the amplitude of the driving force, ω is the angular frequency, k is the spring constant, and c is the viscous damping coefficient. By defining the undamped angular frequency $\omega_0 = \sqrt{k/m}$ and damped ratio $\eta = \frac{c}{2\sqrt{mk}}$, we can rewrite the above equation as

$$\frac{\mathrm{d}^2x}{\mathrm{d}t^2} + 2\eta\omega_0\frac{\mathrm{d}x}{\mathrm{d}t} + \omega_0^2x = \frac{F_0}{m}\sin(\omega t) \tag{2}$$

The general solution of equation (2) is the sum of a transient solution and a steady-state solution. As the transient solution decays very fast, a steady-state solution is sufficient to study the resonance. The steady-state solution takes the following form:

$$x(t) = \frac{F_0}{m\sqrt{(2\omega\omega_0\eta)^2 + (\omega_0^2 - \omega^2)^2}}\sin(\omega t + \phi) \tag{3}$$

where $\phi = \arctan\left(\frac{2\omega\omega_0\eta}{\omega^2 - \omega_0^2}\right) + n\pi$ $(n = 0, 1, 2, \ldots)$

The amplitude of displacement varies depending on the damping ratio (Fig. 2b). Resonance occurs with maximum amplitude at the driving frequency. The resonant frequency ω_r can be obtained as $\omega_r = \omega_0\sqrt{1 - 2\eta^2}$.

Types of acoustic resonances

An open acoustic system interacts and exchanges energy with the surrounding environment. It has a non-Hermitian Hamiltonian and

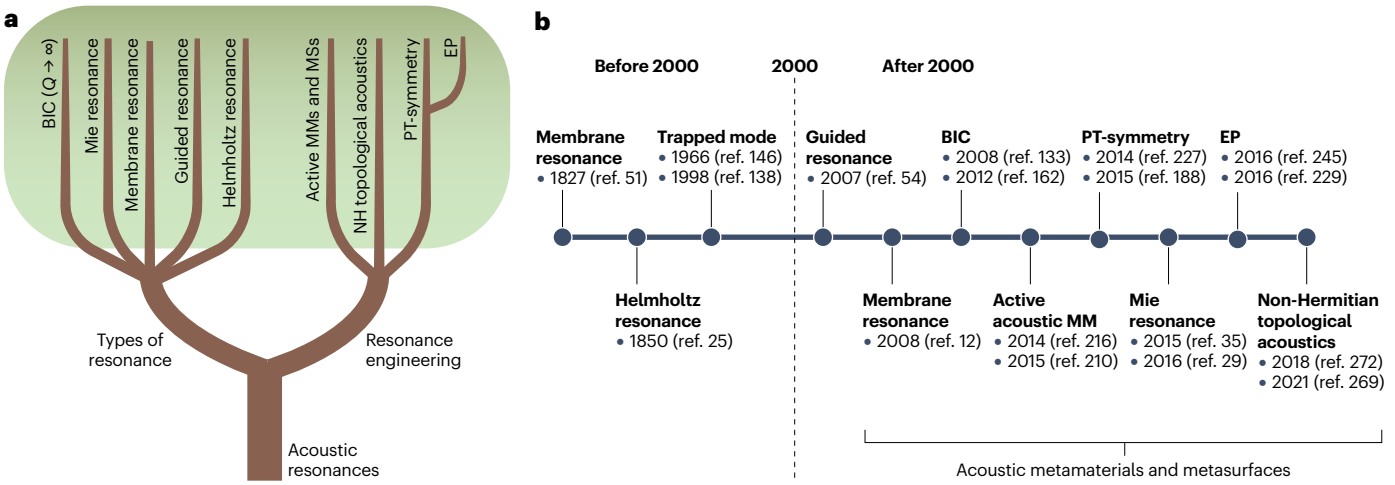

Fig. 1 | Acoustic resonances in non-Hermitian open systems. a, Overview of different types of resonance and ways to engineer them. Acoustic resonances include Helmholtz resonances, Mie resonances, membrane resonances and guided-mode resonances. Bound states in the continuum (BICs) are a unique type of acoustic resonance with infinite *Q*-factors. Acoustic resonances, which are associated with acoustic resonant modes in open systems, can be tailored in an active way or by introducing gain and loss in the coupled resonator system. Exotic topological features also appear in an open system with a tailored non-Hermiticity. **b**, Timeline of milestones in the field. EP, exceptional point; MM, metamaterial; MS, metasurface; NH, non-Hermitian; PT, parity–time.

thus supports a series of acoustic leaky modes[7,8]. Unlike guided modes, whose eigenfields decay exponentially to zero in the far field, leaky modes can propagate into infinity owing to outgoing boundary conditions. These leaky modes[5] are associated with complex eigenfrequencies, which can be written as $\omega = \omega_0 - i\gamma$, where ω_0 and γ are the resonant frequency and radiative decay rate of leaky modes, respectively. Their Q-factors are calculated by the ratio $Q = \omega_0/2\gamma$. Similar to other physical systems, leaky modes in an open acoustic system play a central role in governing its acoustic properties. These resonant states form the basis of many engineered structures such as metamaterials and metasurfaces, which consist specific arrangements of subwavelength resonators.

Helmholtz resonances. Typical examples of acoustic open resonators include musical instruments such as guitars and violins. Amongst these resonators, one of the simplest cases is a Helmholtz resonator, which consists of a rigid-walled, fluid-filled cavity connected to a narrow neck[25]. Helmholtz resonators support many resonant modes, and the fundamental (lowest-order) mode can be modelled as a mass–spring system (Fig. 2c). To a first approximation, the mass of the air in the neck region is given by $m = \rho_0 Sl$, where ρ_0 is the average air density, S is the area of the neck and l is its length. The displacement of the mass of air with cross-section S by distance x leads to a change in the volume of the cavity $\Delta V = Sx$. Consequently, the acoustic pressure p represents the change in pressure relative to its static value, and is related to the change in volume by the adiabatic bulk modulus K:

$$p = K\frac{\Delta V}{V} = K\frac{S}{V}x \tag{4}$$

The restoring force is then the integral of this pressure over the neck cross-section, $F = KS^2x/V$, which is equivalent to Hooke's law for a spring of stiffness $k = KS^2/V$. This effective mass and stiffness act together to form a resonant system, with the resonant frequency given by

$$\omega_0 = \sqrt{\frac{k}{m}} = \sqrt{\frac{KS}{\rho_0 Vl}} \tag{5}$$

Other systems featuring Helmholtz resonances include tube resonators that consist of a tube waveguide connected to a side resonator via a neck. Such open resonators support a series of resonant modes[26], including fundamental and high-order modes[27]. Acoustic BICs are also present when the structure parameters satisfy certain conditions[26]. Helmholtz resonators have been widely used for sound trapping and absorption[28]. They also allow for precise design of the effective bulk modulus. For instance, by arranging an array of subwavelength Helmholtz resonators, an effective dynamic modulus with negative values (rather than the positive values of conventional natural materials) was demonstrated near the resonance frequency in the ultrasonic regime based on the homogenized media theory[11]. This may find promising applications in noise control and emission engineering.

Mie resonances. Mie resonances are typically associated with photons but can also be created in acoustic systems. Similar to Mie resonances in nanophotonics, acoustic multipolar Mie resonances allow tailoring of the far field of acoustic waves. For instance, dipolar Mie resonances can be used for directional sensing[29]. A highly directional and collimated beam without a sidelobe can be realized based on monopolar Mie resonances[30]. Similarly, the radiation pattern can be tailored by placing multiple configurable sources inside the degenerate Mie resonances to achieve enhanced directivity[31]. Mie resonances are usually found in high-index dielectric metastructures[5,32,33], and the emergence of acoustic metamaterials has provided a flexible way to control effective high-index structures for sound.

One strategy for realizing a high refractive index in a single resonator is to coil up the space within it[34]. A maze-like structure can support Mie resonances[35] with monopolar, dipolar and multipolar

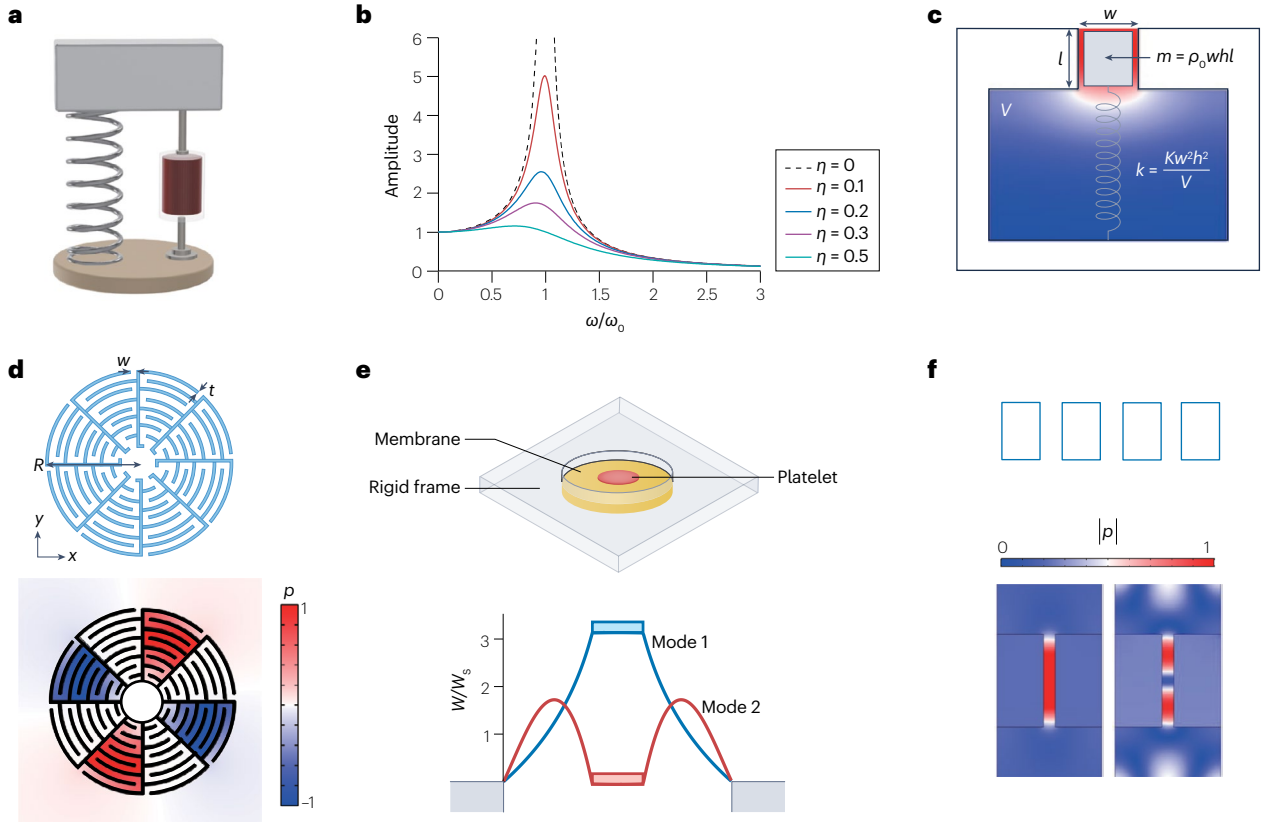

Fig. 2 | Types of acoustic resonance. a, Mass–spring model. **b**, Displacement amplitude versus frequency, ω/ω_o, at different damping ratios, η. **c**, Helmholtz resonator, where the colour gradient denotes the pressure gradient in the cavity. *h*, dimension perpendicular to the page; *K*, adiabatic bulk modulus. **d**, Mie resonator and the pressure-field distribution of quadrupolar Mie resonances. **e**, Membrane resonator and pressure profile of two modes, with W/W_s being the normal displacement of the membrane (W) normalized to the amplitude of the incident sound wave (W_s). **f**, Perforated metallic grating and pressure-field distributions of two Fabry–Perot resonances. Panel **d** adapted with permission from ref. 35, Springer Nature Limited. Panel **e** adapted with permission from ref. 52, Springer Nature Limited.

characteristics (Fig. 2d). The effective high refractive index is obtained in such a structure because the acoustic wave propagates along the zigzag channel, considerably increasing the acoustic path. The high index of the structure also ensures that the dimensions of the Mie resonator fall within the subwavelength regime. The value of the effective refractive index can be easily modulated by controlling the curling number *N* of zigzag channels. For a concentric labyrinthine metamaterial, the complex eigenfrequencies of Mie resonances can be derived in principle by expanding the eigenfunctions in different regions as the superposition of Bessel and Hankel functions, and matching boundary conditions. For other shapes, their complex eigenfrequencies and eigenfields can be calculated by commercial software COMSOL Multiphysics. The nature of Mie resonances can be confirmed by performing multipole decomposition.

If an array of Mie resonators is arranged as an acoustic metasurface in a single chain or 2D lattice, the effective mass density and bulk modulus can be tailored in an unprecedented way. For example, the monopolar and dipolar Mie resonances supported by an ultra-sparse metasurface with a subwavelength thickness induce a single negative bulk modulus and single negative mass density, respectively[35]. Space-coiled metamaterials have been used for realizing simultaneous negative mass density and bulk modulus[34,36,37], and effective impedance can be modulated from a mismatched one to a perfectly matched one with a Mie resonator dimer[38]. Harnessing the fact that the curling number of zigzag channels of Mie resonators controls their effective refractive index, acoustic rainbow trapping has also been achieved[39]. In addition, the widely accessible effective refractive index enables the realization of acoustic gradient-index lenses[40].

Space-coiled acoustic metamaterials with high indices are not the only platform for hosting acoustic Mie resonances. Theoretical work shows that simultaneous negative mass density and negative bulk modulus can be realized by arranging an array of silicone rubber spheres in water[18]. Monopolar and dipolar Mie resonances are usually accompanied by a negative bulk modulus and negative mass density. Double negativity on effective bulk modulus and mass density is observed if both negative responses are strong enough. In 2015, 3D negative refraction was demonstrated by embedding macroporous silicone rubber microbeads in a water-based gel matrix[16]. Such a porous structure reduces the sound speed, pushing the monopolar and dipolar Mie resonances into the low-frequency regime and thereby opening the door to soft acoustic metamaterials[41]. Other metastructures exhibiting multipolar resonances are air bubble arrays in water[42–45], which have been applied to realize extraordinary transmission[46,47], superabsorption[48] and sound focusing[49].

Membrane resonances. Membrane-type or plate-type structures can also host multipolar resonances[3,50]. Compared with 3D-printed metamaterials, decorated membrane resonators[51] are light and thin, and their operation frequency usually falls within the audible range. A membrane resonator consists of a flexible elastic membrane and a rigid platelet attached to the centre of the membrane (Fig. 2e), which can be effectively modelled by a mass–spring oscillator. The typical thickness and diameter of the elastic membrane are submillimetre and several centimetres, respectively. The resonant frequency can be easily tuned by the mass of the rigid platelet. Decorated membrane resonators can tailor the frequency dispersion of mass and bulk modulus. For example, the lowest eigenmode of a membrane resonator exhibits dipolar resonances, which in turn enable the negative density behaviour[12]. When integrated with rigid disks or vibrated higher-order modes, these structures can support monopolar resonances that contribute to a negative modulus[13]. By putting two membrane resonators close to each other, it is possible to realize double negative mass density and bulk modulus, owing to the coupling between them[13]. In addition, perfect absorption has been demonstrated experimentally based on a membrane resonator[52].

Guided-mode resonances. Acoustic resonances can also arise in the form of guided-mode resonances in a periodic array of subwavelength slits or holes perforated in a metallic film (Fig. 2f). Inspired by extraordinary optical transmission in a perforated hole array of a thin metallic film[53], several works independently realized extraordinary acoustic transmission in a grating with a narrow aperture[54,55]. Such an abnormal phenomenon is attributed to the excitation of acoustic guided-mode resonances[56], which interferes strongly with Fabry–Perot resonances in a single aperture. By harnessing the coupling between the evanescent field and Fabry–Perot resonances, acoustic deep-subwavelength imaging was experimentally realized in holey structured metamaterials[57].

Applications of acoustic resonances

Acoustic resonances are a powerful building block for diverse technological applications, which take advantage of their exceptional properties such as enhanced wave–matter interaction, reduced footprint and tunable effective acoustic-material parameters[1,3,58]. Applications range from acoustic narrowband/broadband absorption to vortex beam generation, imaging and enhanced emission.

Acoustic narrowband absorption. Acoustic resonances can enhance sound dissipation over a certain frequency range around the resonant frequencies, thus aiding the development of resonant acoustic absorbers[58–62]. Based on the coupled mode theory[63–65], the reflection coefficient (r) of a resonator in a one-port system can be expressed as

$$r = 1 - \frac{2\gamma}{\mathrm{i}(\omega - \omega_0) + \gamma + \Gamma} \tag{6}$$

where ω represents the angular frequency of the incident waves, ω_0 is the resonant frequency, γ and Γ denote the radiative and dissipative decay rates of the resonance. $\gamma = 1/\tau_r$, and $\Gamma = 1/\tau_a$, with τ_r and τ_a being the lifetimes of the resonance due to radiation and intrinsic (thermoviscous) losses, respectively. The absorption coefficient is then given by $\alpha = 1 - |r|^2$. The interaction between γ and Γ determines the absorption coefficient and gives rise to the 'critical coupling' condition at $\gamma = \Gamma$, leading to a perfect absorption[64,66–70].

When a deep-subwavelength structure in a one-port system supports an acoustic resonance satisfying the critical coupling condition (generally with small γ and Γ), an ultrathin (compared with the working wavelength λ) and narrowband perfect absorber can be achieved[28,71–79]. For example, a membrane-type resonator[52] and a curled-channel resonator[80] have been harnessed to realize narrowband perfect absorption with structural thicknesses below $\lambda/100$ (Fig. 3a).

Acoustic broadband absorption. There are two typical strategies for realizing broadband absorption through the coupling of multiple resonances. The first strategy is to couple resonances that individually approach the critical coupling condition for broadband high-efficiency absorption. Frequently used resonances include quarter-wavelength resonances[81–86], Helmholtz resonances[87–91] and Mie resonances[39,92]. In this strategy, the individual resonances predominantly contribute to the overall absorption performance, for example in an ultra-broadband, high-efficiency absorber whose thickness approaches a minimum[84] (Fig. 3b). In this case, the resonators nearly fulfil the critical coupling condition at their first-order quarter-wavelength resonances.

Another strategy is to couple resonances that individually deviate from the critical coupling condition, and go to an overcoupling regime[93]. This strategy enhances the capacity of the coupling effect[94–97] and enables it to dominate the overall absorption performance[98–106]. Figure 3c manifests a broadband acoustic absorber with minimal thickness by adapting the second design strategy[94]. The Helmholtz resonances individually deviate from the critical coupling condition, and the coupling effect dominates the overall absorption performance.

Acoustic vortex beams. Acoustic vortex beams[107–113] with resonance-based orbital angular momentum have drawn considerable attention in recent years due to their potential for contactless control of objects[114–116] and boosting the capacity of acoustic communication[108,117]. A typical acoustic system that can convert acoustic resonances to orbital angular momentums follows a design with eight fanlike sections of resonators (Fig. 3d). Through the judicious design of the radiation and intrinsic losses of the resonator-pipe systems, target phases of transmitted waves as well as high transmission of incident acoustic waves can be achieved at the resonant frequency, leading to a resonance-based vortex beam with high transmitted energy[107]. Furthermore, the coupled resonances allow for advanced modulation of transmitted waves, paving the way for broadband resonance-based vortex beams[118].

Acoustic imaging. Acoustic resonances find another important application in acoustic imaging for detecting deep-subwavelength features[17,57,119–125]. An array of deep-subwavelength acoustic Fabry–Perot cavities can support the nearly non-dispersive transmission of both propagating and evanescent waves over a wide range of wave vectors at Fabry–Perot resonances, which enables superresolution acoustic imaging with deep-subwavelength ($\sim\lambda/50$) details (Fig. 3e). Nevertheless, the unavoidable intrinsic losses of the Fabry–Perot cavities result in a decreased imaging quality. Comprehensive modulation of both the radiation and intrinsic losses/gains throughout designs may pave the way for improved acoustic imaging[122,123].

Acoustic sources. Acoustic resonances with low radiation (small γ) hold immense potential for enhancing the emission of sound sources

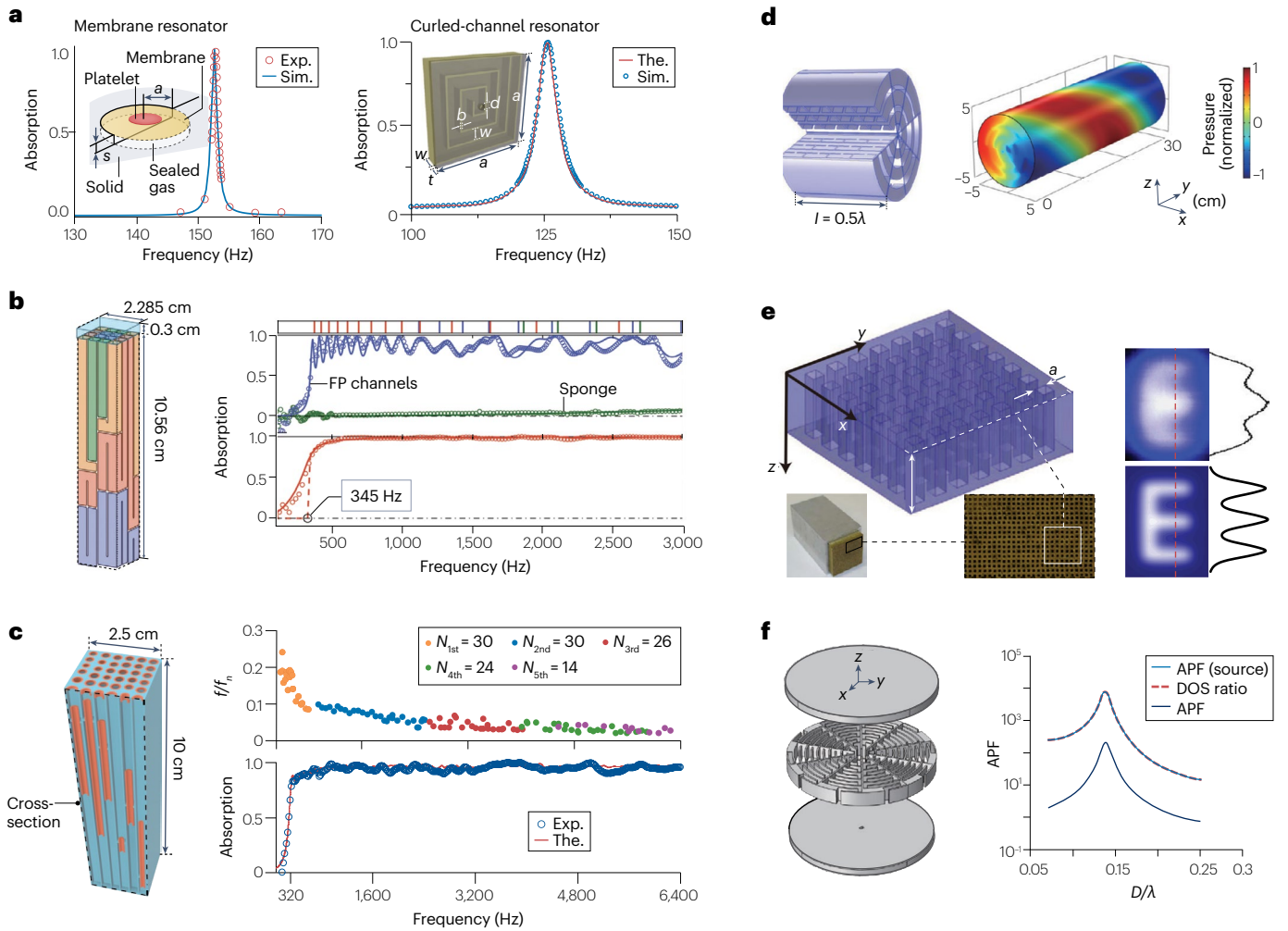

Fig. 3 | Applications of acoustic resonances. a, Acoustic perfect absorbers made of a membrane-type acoustic resonator and a curled-space acoustic resonator. The., theory; Sim., simulation. **b**, Broadband high-efficiency acoustic absorbers consisting of 16 Fabry–Perot (FP) acoustic cavities. Upper right: blue circles, experiment (FP channels); blue line, theory (FP channels); green circles, experiment (sponge); green line, theory (sponge). Lower right: red circles, experiment (FP channels + sponge); red line, theory (FP channels + sponge). Exp., experiment. **c**, Broadband acoustic absorber composed of 36 cascading neck-embedded Helmholtz resonators. **d**, Acoustic vortex beam with resonance-based orbital angular momentum. N_{1st} to N_{5th} denote the orders of the resonances, alongside the numbers of those whose absorption peaks are higher than 0.1; *f* and *fn* represent the theoretical results of the full-width at half-maximum and resonant frequency of a resonance, respectively. **e**, Superresolution acoustic imaging realized by an array of Fabry–Perot acoustic cavities. The stroke width of the letter E is ~λ/50. **f**, Acoustic emission enhancement with Mie resonators. APF, acoustic Purcell factor; DOS, density of states. Left panel **a** adapted with permission from ref. 52, Springer Nature Limited. Right panel **a** adapted with permission from ref. 80, AIP. Panel **b** adapted with permission from ref. 84, RSC. Panel **c** adapted with permission from ref. 94, Oxford Publishing Group. Panel **d** adapted with permission from ref. 107, APS. Panel **e** adapted with permission from ref. 57, Springer Nature Limited. Panel **f** adapted with permission from ref. 126, APS.

such as loudspeakers. This phenomenon is often referred to as the acoustic Purcell effect[126–129]. Mie resonances with low radiation loss offer a promising avenue for achieving emission enhancement[35]. For example, when a loudspeaker is placed at the centre of a structure supporting a Mie resonance, the emitted acoustic waves are amplified compared with emission in free space, particularly around the first-order Mie resonance (Fig. 3f). However, the intrinsic loss within the resonant structure limits the emission enhancement by dissipating the emitted sound waves. A pair of well-matched γ and Γ of an acoustic resonance can induce extreme emission enhancement under a given Γ (refs. 128,129).

Acoustic bound states in the continuum

Acoustic BICs in an open resonator

So far, we have mainly discussed lower-order acoustic resonances with relatively low *Q*-factors. Such acoustic resonances have been widely used in realizing acoustic devices requiring broadband operation, including acoustic absorbers and wavefront shaping. However, for applications such as sensors and filters, high-*Q* acoustic resonances are highly desirable. BICs have been regarded as an ideal platform for realizing high-*Q* acoustic resonances[5,19,20].

The concept of BICs originated from quantum mechanics and was then generalized to acoustics and photonics. Usually, the

continuum spectrum is presented in the form of extended states in continuum frequencies. Outside the continuum, there are some discrete levels, called bound states, that do not support any radiation. Typical examples of bound states include guided modes in an optical fibre and defect modes in a photonic bandgap structure. Inside the continuum, a series of leaky resonances appear, due to the coupling of bound states with the continuum. BICs correspond to perfectly trapped modes with forbidden radiation despite embedding into the continuum spectrum. Strictly speaking, BICs cannot be accessed by any external excitation because they are completely decoupled from the radiation waves despite outgoing boundary conditions. Mathematically speaking, a BIC corresponds to a resonant mode with zero radiative decay rate and infinite Q-factor, which is $\omega = \omega_0 - i\gamma$ ($\gamma = 0$, $Q = \omega_0/2\gamma = \infty$).

Symmetry-protected BICs. If a system obeys reflection or rotational symmetry, some eigenmodes become symmetry-protected BICs owing to symmetry incompatibility[19,26,130,131]. A simple system hosting symmetry-protected BICs consists of a circular or rectangular rigid obstacle in the centre of a waveguide with hard boundaries[27,132–139]. The typical symmetry-protected BIC in such a system has an eigenfield profile that is antisymmetric with respect to the x-axis (Fig. 4a, top).

Another excellent platform for studying BICs is a coupled waveguide–resonator system. For example, if two waveguides are attached symmetrically to the centre of the left and right sides of rectangular resonators, a series of symmetry-protected BICs are supported[26,130]. Two typical symmetry-protected BICs are modes M_{12} and M_{22}, both of which show antisymmetric pressure-field distributions (Fig. 4a, middle). The underlying physics behind such BICs is revealed by applying an effective non-Hermitian Hamiltonian method[7,8,130,140–145] (Supplementary Sections 1.1 and 1.2).

Breaking the symmetry results in the transition from BICs into quasi-BICs with a finite Q-factor. As the symmetry is broken, the Q-factor is inversely proportional to α^2, where α is the asymmetry parameter of the system (Fig. 4a, bottom). Symmetry-protected BICs (Fig. 4a, top) were experimentally verified in 1966[146], and quasi-BICs (Fig. 4a, middle) have recently been demonstrated experimentally, thanks to the advance of 3D printing technology[26,147]. A recent study[148] revealed that symmetry-protected BICs can be sustained in a coupled cylindrical waveguide–cuboid resonator as long as the project-plane symmetry is satisfied, further relaxing the usual requirement of building symmetry-protected BICs that the attached waveguide should share the same cylindrical axis.

Accidental BICs. Previous studies showed that a photonic crystal slab or dielectric metasurface supports accidental BICs in the first Brillouin zone[149]. However, one cannot define the first Brillouin zone in a finite system, such as a coupled waveguide–resonator system (Fig. 4b). Under such circumstances, accidental BICs are constructed by moving the position of the attached waveguides[150,151]. Taking a single-port coupled waveguide–resonator system as an example (Fig. 4b, top), zero coupling ($W_{mn;p=1} = 0$) between propagating mode of waveguide and eigenmode M_{mn} happens at

$$a = \frac{2s-1}{2(n-1)}L_y - \frac{1}{2}, \text{ with } s = 1, 2, 3, \ldots, n-1 \quad (7)$$

if only the first channel $p = 1$ is considered. Note that this equation gives the critical position around which the BICs are found. For an even n, symmetry-protected BICs occur exactly at $a = (L_y - 1)/2$. Accidental BICs only happen at $n > 2$. The pressure-field distributions of two typical accidental BICs are almost the same as the eigenfield distribution of mode M_{13} in a closed resonator (Fig. 4b, middle). Nevertheless, the critical position of the attached waveguide for accidental BICs always slightly deviates from the above prediction because of the contribution of evanescent modes (Fig. 4b, bottom). Other accidental BICs are found by tuning the angle between two waveguides in a non-axisymmetric cylindrical waveguides[148,152]. Note that the formation physics of accidental BICs is also well captured by the effective non-Hermitian Hamiltonian method[148,150–152] (see Supplementary Section 1.2).

Friedrich–Wintgen BICs. Friedrich–Wintgen BICs are a type of non-trivial BICs that have triggered extensive interest in both acoustic and photonic communities (Fig. 4c). The fundamental physics behind Friedrich–Wintgen BICs are the interferences between resonant modes[153], which can be described by a simplified two-mode approximation system[154,155] (Supplementary Section 1.3). When the eigenenergies of two resonant states cross each other with a continuous parameter, strong mode coupling directly leads to the avoided crossing of two modes in the eigenenergy space[156]. Meanwhile, the resonance linewidth of one mode is reduced to zero, signifying the formation of BICs, and the other is boosted to maximum[157]. Thus, the key to realizing Friedrich–Wintgen BICs is to build avoided crossing of two leaky modes as a function of a continuous parameter. For a rectangular resonator with two waveguides symmetrically attached, one can always find Friedrich–Wintgen BICs by considering a pair of modes M_{mn} and $M_{m+2,n-2}$ via tuning the size ratio between height and width, because these two modes become degenerate at a certain size ratio for a closed rectangular resonator[26,130]. The attached open waveguides introduce strong coupling between the modes, leading to the avoided crossing of the modes' resonance position and formation of Friedrich–Wintgen BICs. The strategy of creating avoided crossing of pair modes has been widely used to construct quasi-BICs or BICs in a single dielectric particle system or an array of such systems[158,159]. Here, it is noteworthy that when constructing Friedrich–Wintgen BICs, two modes must have the same parity so that their eigenfield distributions can evolve into each other. In principle, pair eigenmodes M_{mn} and $M_{m+1,n-1}$ in the closed resonator can become degenerate at a specific size ratio even if they have opposite parity. These pair modes can also be applied to build Friedrich–Wintgen BICs in a more general way[150]. For example, modes M_{21} and M_{12} become degenerate at $R = 1$. On introducing one or two semi-infinite waveguides and varying the dimension of the resonator, one of the eigenmodes becomes Friedrich–Wintgen BICs[150,153] (Fig. 4c, bottom). The interesting thing is that the eigenfield of Friedrich–Wintgen BICs is a superposition of eigenmodes M_{21} and M_{12} of a closed resonator. Tuning the attached waveguide position can help to arbitrarily engineer the eigenfield distribution of Friedrich–Wintgen BICs. The nature of the BICs can also be switched from Friedrich–Wintgen BICs to accidental BICs or symmetry-protected BICs by moving the waveguide position.

Fabry–Perot BICs. When two identical resonators are coupled to each other via the same waveguide channel, Fabry–Perot BICs are found by tuning the distance between them[160–163]. The formation mechanism is well captured by a simple two-level system (Supplementary Section 1.4). Each resonator serves as a perfect mirror on resonance. When the propagating phase ϕ satisfies $\phi = kd = m\pi$ ($m = 1, 2, 3\ldots$), acoustic waves are perfectly trapped between two mirrors, and thus bonding or

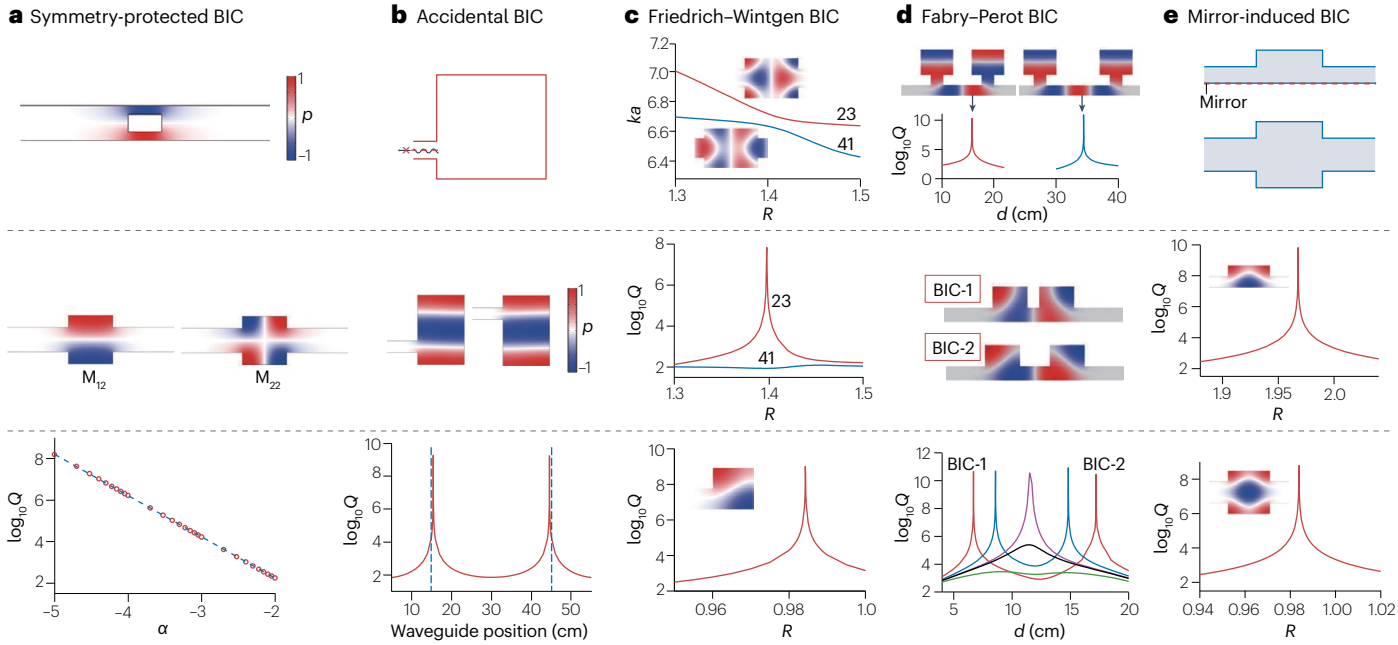

Fig. 4 | Acoustic BICs. a, Typical eigenfield distribution of symmetry-protected bound states in the continuum (BICs) and the *Q*-factor of quasi-BICs versus asymmetry parameter α. **b**, Accidental BICs. The top panel shows a schematic drawing of a single-port waveguide–resonator system. The middle panel shows the eigenfield distributions of two representative accidental BICs. The bottom panel shows the *Q*-factor versus attached waveguide position. **c**, Friedrich–Wintgen BICs in a coupled waveguide–resonator system. The top and middle panels correspond to the normalized resonant frequencies (ka) and *Q*-factors of modes M_{23} and M_{41} versus the size ratio R of the rectangular resonator. The bottom panel shows the *Q*-factor of twisted mode M_{12} as a function of size ratio. **d**, Fabry–Perot BICs in a coupled waveguide–dimer resonators system. The top panel shows the eigenfield distribution of normal Fabry–Perot BICs and their *Q*-factors versus distance d between two resonators. The middle panel shows the eigenfield distributions of two antibonding Fabry–Perot BICs before merging. The bottom panel shows the *Q*-factors of antibonding Fabry–Perot BICs versus distance before and after merging. **e**, Mirror-induced BICs in a coupled waveguide–resonator system. The top panel shows the schematic drawing of side-coupled waveguide–resonators and their equivalence of coupled waveguide–rectangular resonators. The middle and bottom panels show the *Q*-factors versus the size ratios of side resonators and rectangular resonators. Panel **b** adapted with permission from ref. 150, APS. Bottom panel **c** adapted with permission from ref. 150, APS. Panel **d** adapted with permission from ref. 164, Wiley.

antibonding Fabry–Perot BICs are formed (Fig. 4d, top). Note that the resonators are coupled with the waveguide through a short neck. If the neck is removed, two bonding (antibonding) Fabry–Perot BICs appear, and they move, merge and disappear (Fig. 4d, middle and bottom) as a function of distance between coupled resonators as the width of the rectangular resonator is varied[164]. Unlike merging BICs occurring in momentum space in a dielectric grating[165] or photonic crystal slab[166], such a BIC merging phenomenon was found in geometry parameter space, considerably relaxing the fabrication errors. This unique phenomenon is explained from a topological charge evolution perspective, where each BIC is correlated to a pair of +1 and −1 charges.

Mirror-induced BICs. Because the exterior boundaries of most acoustic resonators are set as hard walls, equivalent to the perfect electric conductor in electromagnetics, it is reasonable to treat them as partial mirrors (Fig. 4e). Under such circumstances, all BICs whose eigenfield profile is symmetric with respect to the certain axis can be converted into mirror BICs by reducing the dimensions to half the original size[26]. The shrunk dimensions also reduce mode volume and enhance the Purcell effect in acoustics. The mirror-based approach provides researchers with an easy and straightforward way of building more BICs.

Applications of acoustic BICs

Acoustic BICs allow for the realization of high-*Q* acoustic resonances, offering a new platform for developing acoustic devices featuring high intensity and high sensitivity. Many acoustic applications based on normal Fabry–Perot resonances, Helmholtz resonances and Mie resonances can find counterparts based on acoustic quasi-BICs, and the quasi-BICs can further push the performance limit of some acoustic devices that other normal resonances cannot offer, such as higher sensitivity, higher energy intensity and enhanced wave–matter interactions.

Perfect absorption. Acoustic quasi-BICs have an ultra-small radiation loss (γ), and thus narrowband perfect absorption can be achieved for acoustic quasi-BICs when fulfilling critical coupling with a matched intrinsic loss (Γ). When two quarter-wavelength cavities have the same cross-section and the same cavity length, a pure BIC can be achieved (Fig. 5a). By introducing a small length difference (Δl) between the two cavities, a quasi-BIC with low and tunable radiation loss can be realized. In conventional wisdom, wide cavities are considered ineffective for sound absorption owing to their low intrinsic loss. In fact, perfect absorption can be realized with a pair of balanced low intrinsic and radiation losses[147]. Although the two cavities show very low absorption individually, together they achieve coherently perfect absorption with

strong pressure-field enhancement (Fig. 5b). Note that this concept can also be applied in other fields of wave physics such as elastic-wave systems[167,168]. Additionally, chiral absorptions of vortex beams with specific orbital angular momentum have been reported in systems harnessing the chiral quasi-BIC, manifested by perfect absorption of a left-handed incident vortex and total reflection of a right-handed counterpart[169]. The chiral quasi-BICs are induced by breaking mirror symmetry along the azimuthal direction.

Acoustic emission enhancement. Acoustic quasi-BICs are the ideal candidates for pursuing large acoustic emission enhancement owing to the easily accessible infinitesimal radiation loss. Quasi-BIC-induced acoustic emission enhancement has been demonstrated recently by placing a loudspeaker at the bottom of an acoustic quasi-BIC-supporting system[129]. In the absence of the intrinsic loss (Γ), a quasi-BIC with decreasing radiation loss (γ) induces increasing emission enhancement, and an infinitesimal γ leads to infinitely large emission. However, the intrinsic losses in practical acoustic systems weaken the emission enhancement, so the γ of a quasi-BIC needs to be tuned to approach the value of Γ to maximize the emission enhancement under a given Γ. For a sample with a square cross-section of 100 mm side length, the maximum acoustic Purcell factor[126] achieved is 84.7 at the quasi-BIC[129] (Fig. 5c). The maximum acoustic Purcell factor can be enhanced by reducing the intrinsic loss of the quasi-BIC-supporting system.

Active phononic metamaterials and metasurfaces

Although passive acoustic resonances offer versatile ways to leverage sound–matter interactions, it is highly desirable to implement their tunability and reconfigurability in practical applications. The fast development of phononic metamaterials has mainly relied on resonances in systems made of passive, linear time-invariant inclusions, as discussed above. The passive phononic metamaterials, albeit providing more straightforward designs, inevitably come with strong physical constraints, such as causality, passivity and reciprocity, for the corresponding achievable effective properties[1,3,170,171]. Notably, causality yields the Kramers–Kronig relations[172], which fundamentally limit the operating bandwidth of these devices, while inherent dissipation, such as thermoviscous damping of airborne sound, strongly hampers their efficiency. These properties are particularly restrictive in the case of resonant inclusions, building blocks of a considerable number of metamaterial designs for which a trade-off between size and operating bandwidth usually occurs.

In response to these various obstacles, active phononic metamaterials provide new opportunities that have been extensively explored in the past 10 years, allowing the breaking of causality, passivity and reciprocity[1,3,65,173,174]. By definition, active metamaterials encompass systems with some of the following properties: non-passivity, nonlinearity and time-dependence. Their building blocks are achieved through various techniques such as piezoelectric patches[175–179] for sound and elastic waves, electromagnet actuators[180–183], motorized moving parts[184–187], electronic circuitry involving loaded elements[188–190] or feedback control[191–197], active fluids[198,199], thermoacoustic effects in carbon nanotubes[200,201], advanced additive manufacturing techniques for magneto[202,203] and ultraviolet light-responsive material[204], and devices harnessing air ionization properties[205]. At the chip scale, the addition of d.c. gate voltage[206], micro/nanoelectromechanical actuators[207,208] and optomechanical devices[209] have also been investigated.

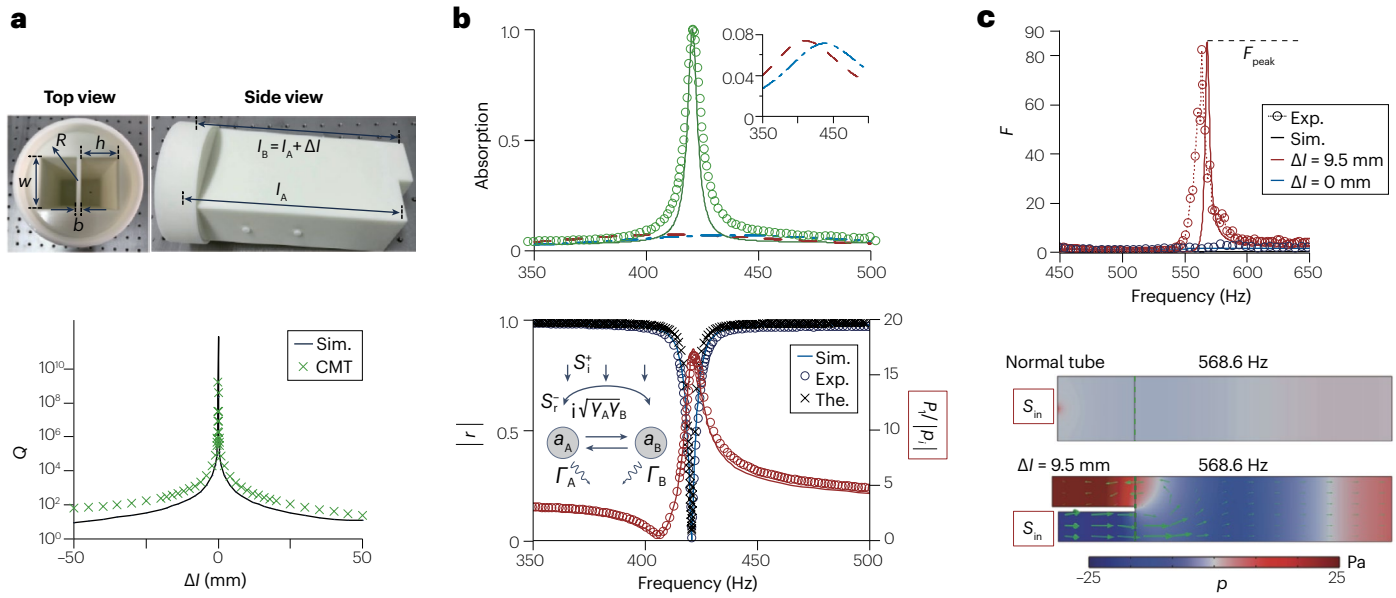

Fig. 5 | Applications of acoustic BICs. a, Example of a Friedrich–Wintgen BIC-supporting system consisting of two acoustic quarter-wavelength cavities, and the calculated and simulated Q (without intrinsic loss) for varying Δl. CMT, coupled mode theory. **b**, The top panel is the absorption coefficients of the coherent system (green), individual cavity A (blue) and individual cavity B (red). The bottom panel is the reflection factor (blue) and pressure amplification (red). γ, radiation loss; Γ, intrinsic loss; P_1, pressure amplitudes at point 1 referring to ref. 147; $|p_i|$, pressure amplitudes of incident waves; S_i^+ and S_r^- represent incident and reflected waves, respectively; a_A and a_B denote the mode amplitudes of cavities A and B, respectively. **c**, Measured and simulated acoustic Purcell factors, F, and simulated acoustic pressure distributions of a normal (empty) tube and the presented two-state system. S_{in} denotes the sound source. Panels **a** and **b** adapted with permission from ref. 147, APS. Panel **c** adapted with permission from ref. 129, Elsevier.

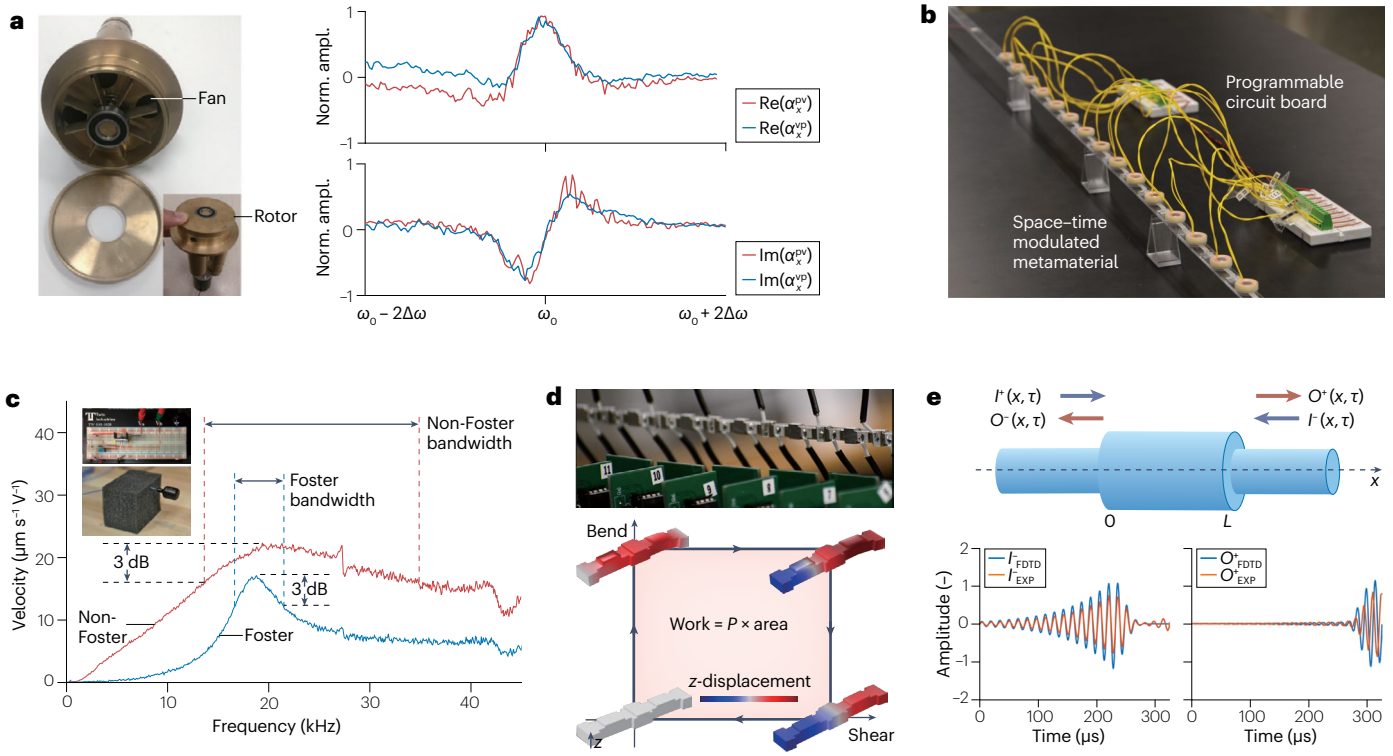

Fig. 6 | Active acoustic and phononic metamaterials. a, Meta-atom with odd Willis parameter for non-reciprocal scattering obtained thanks to internal flow control. The terms α_x^{pv} and α_x^{vp} are Will coupling coefficients that indicate the cross-coupling polarizability. **b**, Spatiotemporal modulated elastic beam for non-reciprocal transmission. **c**, Non-Foster circuit-based acoustic radiation from an active piezoelectric transducer. **d**, A beam with a collection of sensors and actuators presents odd elasticity behaviour allowing for work extraction. **e**, Virtual coherent absorption for elastodynamic waves. $I(x,\tau)$ and $O(x,\tau)$ denote magnitude of incoming and outgoing fields. Panel **a** adapted with permission from ref. 185, Springer Nature Limited. Panel **b** with permission from ref. 181, APS. Panel **c** adapted with permission from ref. 189, National Academy of Sciences USA. Panel **d** adapted with permission from ref. 218, Springer Nature Limited. Panel **e** adapted with permission from ref. 222, AAAS.

Despite the inherent issues of stability and energy of these active schemes, several exciting properties have been achieved with actively tunable phononic resonances and metamaterials. For instance, a reconfigurable electroacoustic metasurface allows real-time sonic steering for possible applications in sensing and communications[210]. On a larger scale, a wall whose building blocks are two-state reconfigurable elements consisting of membranes loaded with magnets allows enhanced spatiotemporal control of the acoustic field in a room, both in the transient and stationary regime[180,211]. Moreover, proper design of active components can break time-reversal symmetry in the system by inducing temporal modulation or putting the medium into motion, achieving non-reciprocity[178,184,212–215]. For instance, a geometrically symmetric resonant meta-atom with an embedded fan shows non-reciprocal scattering, which can be interpreted as an odd Willis coupling parameter under time-reversal symmetry[185] (Fig. 6a). Besides, the spatiotemporal modulation of a linear elastic beam loaded with magnetically tunable resonators generates asymmetric band structures, yielding non-reciprocal wave transmission[181] (Fig. 6b). Active components can also induce tailored nonlinearities in the medium to break phononic reciprocity[216,217] or mimic biological systems[195].

Furthermore, active media can be designed to induce controllable gain or loss in passive systems. For example, the active addition of gain to passive resonances can enhance their radiated power and greatly increase their bandwidth without changing their size, as demonstrated with an acoustic antenna linked to a piezoelectric non-Foster circuit[189] (Fig. 6c). Such active properties also permit the practical implementation of an elastic beam with odd elasticity, allowing for wave propagation in overdamped media and work extraction[218,219] (Fig. 6d). Finally, going beyond the addition of physical gain or loss, it is possible to make passive resonant systems behave as if they had these non-Hermitian features by precisely tailoring the temporal shape of the impinging wave[220,221]. These 'virtual excitation' protocols allow for coherent absorption of elastodynamic waves[222] (Fig. 6e).

Non-Hermitian acoustics and phononics

PT-symmetry and EPs in non-Hermitian systems

Active phononic metamaterials and metasurfaces offer a viable path to exploring fascinating non-Hermitian systems. Additionally, extending acoustic resonances into the non-Hermitian regime can be linked to PT-symmetry and EPs with tailored non-Hermiticity. In the parameter space (usually the onsite loss or gain), a balanced loss–gain modulation can lead to the formation of an EP, which is a close analogy of the PT-symmetric system originally proposed in quantum mechanics[223–226]. Details on the theoretical background and mathematical description can be found in Supplementary Section 2. Early works of PT-symmetry and EPs in non-Hermitian acoustic systems focused on strictly balanced

loss and gain media[227,228]. Owing to the absence of natural gain media, experimental approaches[188,229–231] usually exploit active components such as loudspeakers. Conversely, loss is typically realized by natural dissipation associated with porous materials or groove structures. PT-symmetry and the access of EPs are manifested by unidirectional zero reflection of the system, where incident waves are reflectionless in only one direction. Another attractive application of PT-symmetry is the invisibility cloak[227], experimentally verified using non-Foster electrical circuits[188] and metasurfaces[232].

Along with the efforts to synthesize acoustic gain media[233], researchers have also worked on purely passive structures that support PT-symmetry ('passive PT-symmetry')[234–236]. These purely passive systems in which only loss takes place can induce phenomena similar to those existing in a balanced gain–loss system. For example, non-Hermitian degeneracies of the eigenvalues were observed in 1D wave systems[234,235], later extended to 2D systems[237,238]. Unidirectional sound focusing can arise from a 2D curved metamaterial crystal at the transition point between unbroken and broken PT-symmetry phases (Fig. 7a). These concepts are also extended to metasurfaces, where different diffraction orders are mapped to the specific ports in 1D or 2D systems. As a result, strongly asymmetric diffraction[239–241] and higher-order EPs[242] are observed by tuning the intrinsic loss of the metasurfaces. Combining PT-symmetry and nonlinear effects can further lead to the realization of other intriguing phenomena, including acoustic non-reciprocity[243,244].

Another way to synthesize EPs is to use coupled resonator systems, which offer the convenience of engineering the onsite energy, cross-coupling and intrinsic loss that can be directly mapped to the Hamiltonian of the system. In addition to a single EP which can be realized in two coupled resonators, more complex non-Hermitian physics and higher-order EPs are found in a multiresonator system[245] (Fig. 7b). This approach has received much research attention in recent years,

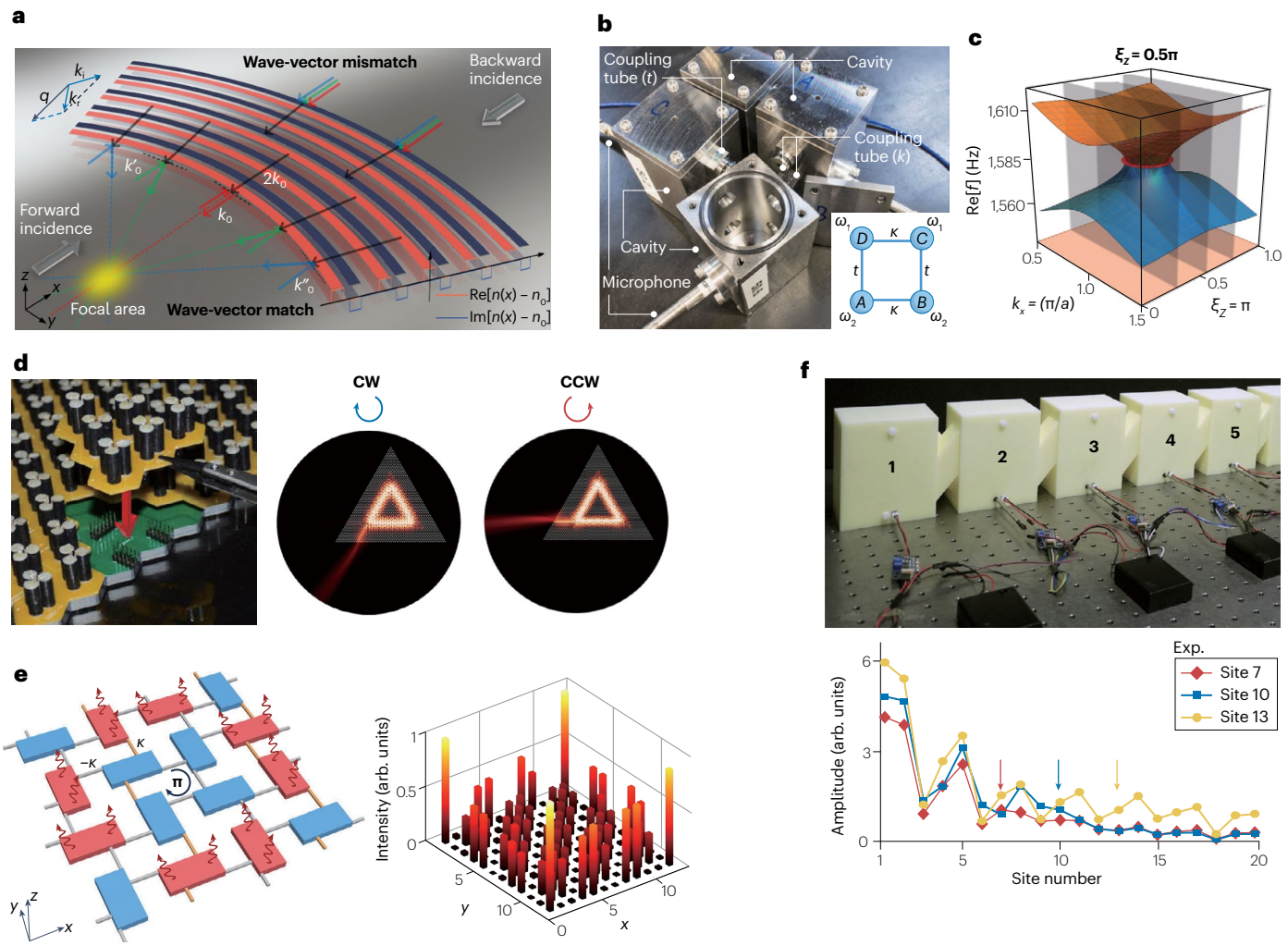

Fig. 7 | Non-Hermitian acoustics and phononics. a, An all-passive acoustic parity–time-symmetric metamaterial for unidirectional wave focusing. **b**, Higher-order exceptional points arising from four coupled acoustic cavity resonators. **c**, Synthetic Weyl exceptional rings in a non-Hermitian phononic crystal. **d**, Non-Hermitian topological whispering gallery modes allowing for audio lasing with selective chirality. **e**, Non-Hermitian induced higher-order topology. **f**, Sonic non-Hermitian skin effect in a chain of actively coupled acoustic cavities. Panel **a** adapted with permission from ref. 237, APS. Panel **b** adapted with permission from ref. 245, APS. Panel **c** adapted with permission from ref. 254, APS. Panel **d** adapted with permission from ref. 269, Springer Nature Limited. Panel **e** adapted with permission from ref. 276, Springer Nature Limited. Panel **f** adapted with permission from ref. 282, Springer Nature Limited.

Glossary

Acoustic Purcell factor
Acoustic Purcell factor is defined as the ratio of emitted acoustic power of an acoustic source in a structure and in free space (or in an empty tube for waveguide systems).

Active acoustic systems
Active acoustic systems involve tunable properties including non-passivity, nonlinearity and time-dependence.

Bound states in the continuum
Bound states in the continuum (BICs) are peculiar states with infinite quality factors (or lifetime) and forbidden radiation, despite residing in the radiation continuum.

Fabry–Perot resonances
Fabry–Perot resonances usually occur in a cavity made of two parallel reflecting surfaces. They appear only when the accumulated round-trip phase in the cavity equals an integer number of 2π.

Hermitian system
A Hermitian system is usually associated with a closed system with a Hermitian Hamiltonian satisfying $H=H^{+}$, where + indicates the combination of complex conjugation and transposition of Hamiltonian. The Hermitian nature ensures real eigenvalues and orthogonal eigenvectors.

Non-Hermitian system
A non-Hermitian system has a Hamiltonian that is not equal to its conjugate transpose, $H\neq H^{+}$, giving rise to complex eigenvalues and non-orthogonal eigenvectors, manifested by an open system that involves interaction and energy exchange with the surrounding environment.

Passive acoustic systems
Passive acoustic systems rely on the natural propagation and reception of sound waves without any intentional modification or manipulation.

Q-factors
The Q-factor is defined as the ratio of the stored energy to the dissipated energy per radian of the oscillation. It is widely used to describe the resonance behaviour of an underdamped harmonic oscillator.

Quasi-bound states in the continuum
Quasi-bound states in the continuum correspond to the eigenstates with finite but high-quality factors by perturbing system from critical parameters.

Willis coupling
Willis coupling in acoustic materials defines the coupling strength between strains and momentum, analogous to bianisotropy in electromagnetics.

with many unusual properties demonstrated, including but not limited to anisotropic EPs[246], enhanced sound absorption[78,247,248], chirality reversal[111,249], topological properties[250,251] and so on[252,253]. For instance, a continuous enclosed trajectory of EPs can form an exceptional ring that enables the exploration of high-dimensional non-Hermitian physics[254] (Fig. 7c). Along this line, the unique topology of EPs arising from non-Hermitian systems is also studied in the context of various acoustic resonator structures[255–257].

Non-Hermitian topological acoustics and phononics

EPs yield non-zero topological charge which can be directly probed thanks to the direct tuning of dissipation and coupling strength enabled by resonant acoustic metastructures[245,250,251,254], hereby introducing a topological description of these non-Hermitian acoustic and elastic resonant systems. The practical implementation of phononic topological insulators[24,199,258–261] based on the Hermitian bulk–boundary correspondence often depends on active building blocks to break time-reversal symmetry and induce the topological order[206]. In this context, acoustic Floquet topological devices have been proposed as non-reciprocal sonic leaky-wave antennas[262]. Moreover, substantial efforts have been made to extend topological band theory to non-Hermitian phononic systems, offering exciting opportunities beyond the usual Hermitian picture. Owing to the complex nature of the energy diagram, non-Hermitian bandgaps are fundamentally different from their Hermitian counterparts. By definition, bandgaps are ensembles of complex eigenvalues that do not intersect any of the bands in the complex plane, which can be either line gaps or point gaps[263,264] associated with inherently distinct features in the non-Hermitian context. Here we describe some recent phononic implementations related to these bandgaps, but we encourage curious readers to check the recent literature[263–266] for a more complete description of these phenomena.

The first approach to implement non-trivial line-gap topology consists of adding loss and gain within the building blocks of a Hermitian topological insulator. The resulting non-Hermitian topology of the bandgap can be described by a non-zero topological invariant[267], corresponding to damped and amplified edge modes which have been studied in the context of valley-Hall[268,269] and higher-order phononic topological insulators[270,271]. For example, the thermoacoustic effect of carbon nanotubes has been used to induce gain within a cavity based on valley interface states, and demonstrated the equivalent of audio lasing with embedded chirality[269] (Fig. 7d). Besides, quasi-periodically arranged resonators on an acoustic tube with controlled dissipation yield topological edge states related to EP properties[272]. Moreover, non-trivial topological bandgaps can be solely opened by adding loss or gain to the medium[273–275]. Notably, by tailoring the spatial arrangement of absorbers within a 2D lattice of acoustic cavities, it is possible to open trivial and topological bandgaps hosting corner modes in a controllable manner[276] (Fig. 7e).

If line-gap topology can be somehow related to Hermitian counterparts, the case of point gaps is fundamentally different and intrinsically non-Hermitian. Typically, point-gap topology is described by the winding number of complex bands instead of eigenvectors, which results in wavefunctions with a net flow towards a specific direction of space[277,278]. Adding an open boundary to the medium in that direction leads to the accumulation of bulk wavefunctions at the edge boundary, known as non-Hermitian skin effects[267,279–281]. Such effects have been realized experimentally in acoustics within a 1D lattice of resonant cavities with asymmetrical couplings induced by active components[282] whose fine-tuning can generate several types of winding topology (Fig. 7f). Similar phenomena have been induced by complex excitations[283], transposed to higher-order schemes[284] and studied in active elastic media[285–288].

Outlook

The recent emergence of acoustic metamaterials and metasurfaces has provided attractive platforms for tailoring acoustic wave propagation in unprecedented ways. The past two decades have witnessed rapid progress in accurately controlling acoustic resonances and developing them towards applications ranging from noise control to subwavelength imaging. Despite much progress made in this field, many questions remain unanswered, and numerous opportunities are awaiting exploration.

So far, most resonance-based acoustic devices, such as those used for vortex beam generation, subwavelength imaging and source emission enhancement, have been limited to relatively narrowband operation due to the dispersion nature of resonances. This narrowband limitation poses a challenge in expanding their practical implementation. Recent research on resonance-coupled

acoustic absorbers has provided fresh insights into broadening the operating frequency bandwidth, which may inspire the development of other resonance-based acoustic devices. Furthermore, although resonance-based acoustic devices demonstrate exceptional performance in laboratory settings, their performance could be limited by various factors in real-world application environments, including high-intensity sound, airflow, low temperature and restrictions imposed by mechanical and material properties. Hence, future efforts should be directed towards investigating resonance-based acoustic devices involving complex environmental factors.

Acoustic BICs have been intensively investigated in an open resonator in the past decade. Because both BICs and EPs correspond to singular states, it is worthwhile investigating EPs in such an open system and revealing their connection with BICs. Coupled waveguide–resonator systems provide additional freedom to control acoustic resonances, giving rise to Fabry–Perot BICs. Merged BICs also have been reported. What will happen if the number of resonators is further increased? If an array of coupled resonators is placed along a waveguide, we may find unique topological properties that are tightly bonded to BICs. Also, it would be useful to develop merged BICs in a single resonator, which would reduce the size of the system. In addition, as BICs reported so far are all passive, it is desirable to realize active BICs for real applications. Another direction worth investigating is acoustic BICs in a periodic system. Many interesting designs in photonic BICs can be directly transplanted to acoustic metasurfaces, offering increased flexibility in tailoring acoustic waves.

On the application side, only a few devices using BICs have been proposed. We expect that there will be more research effort to push the practical application of BICs. For example, it is possible to design chiral acoustic metamaterials and unidirectional emissions in either a single or periodic system by exploiting the singularity of BICs. Additionally, it seems plausible to build a sound laser based on high-Q quasi-BICs. Although so many future opportunities exist, the maximum Q-factor of a quasi-BIC is bounded by the thermoviscous loss in real systems, which in turn limits the largest pressure-field enhancement, preventing the realization of high-performance acoustic sources. Understanding how to alleviate the effect of viscous loss still remains a challenge for pushing the upper limit of measured Q-factor to a few thousand or even more. A recent study on non-Hermitian topological whispering gallery[269] suggests that incorporating gain medium into resonators may be a good solution to this issue.

Furthermore, active metamaterials have introduced extreme degrees of reconfigurability, enabling the dynamical steering of sound and the optimization of its spatial profile. Their non-passive, nonlinear and time-dependent properties, implemented with a broad range of devices, allow wave manipulation beyond that which passive resonances can offer. Hence, broadband, non-reciprocal and enhanced acoustic wave propagation phenomena have been demonstrated, opening new avenues for signal control and steering from the macroscale to the microscale. Nevertheless, inherent issues of stability, speed, synchronization and potentially bulky circuitry are technical challenges that must be addressed to reduce the footprint of such active metamaterials.

Although investigations on PT-symmetric systems and EPs in coupled resonator systems have revealed an interesting correlation between the eigenstate of a system and its response to external excitations, an ongoing effort is to push these studies into higher dimensions or synthetic dimensions. This could lead to the realization of more complex systems with richer physics, and the versatile engineering of EP trajectories in parameter space. Finding practical applications is another promising direction in this field. For example, it has been shown that a greater sensitivity can be achieved by leveraging higher-order EPs. PT-symmetric systems can also give rise to macroscopic asymmetric wave-scattering effects. Along this line, we envisage that the engineering of non-Hermitian PT-symmetric and EP-based systems by harnessing their interaction with the environment could lead to exciting possibilities in wave physics. Nevertheless, challenges remain in realizing EPs in complex resonator systems, especially those with exotic topologies. For example, tuning the parameter space in a highly coupled platform could be difficult as the resonance states are sensitive to perturbations. Also, it is still not an easy task to design EP-embedded structures with practical relevance and scalability for real-world applications.

Adding non-Hermitian features to the tight-binding Hamiltonian opens many new opportunities in the context of topological band theory. Notably, fundamental questions related to the topological description of non-Hermitian systems still need to be answered, particularly in relation to the bulk–edge correspondence and to systems with higher dimensions. Resonant metastructures provide a powerful platform to investigate these fundamental topological effects before their potential generalization to other wave domains, such as microwaves, photonics or polaritonics. On the practical side, a deeper understanding of non-Hermitian topological systems may help to improve the performance of robust devices whose properties go beyond what Hermitian topological systems can achieve. In particular, on their translation to chip-scale footprints, these non-Hermitian topologically protected effects may enable phononic lasing and directional field enhancement mediated by the non-Hermitian skin effect, opening opportunities for advanced telecommunications and sensing, once the technical challenges related to instabilities and fabrication accuracy have been addressed.

Published online: 21 November 2023

References

1. Cummer, S. A., Christensen, J. & Alù, A. Controlling sound with acoustic metamaterials. *Nat. Rev. Mater.* **1**, 16001 (2016).
2. Assouar, B. et al. Acoustic metasurfaces. *Nat. Rev. Mater.* **3**, 460–472 (2018).
3. Ma, G. & Sheng, P. Acoustic metamaterials: from local resonances to broad horizons. *Sci. Adv.* **2**, e1501595 (2016).
4. Rotter, I. & Sadreev, A. F. Avoided level crossings, diabolic points, and branch points in the complex plane in an open double quantum dot. *Phys. Rev. E* **71**, 36227 (2005).
5. Huang, L., Xu, L., Powell, D. A., Padilla, W. J. & Miroshnichenko, A. E. Resonant leaky modes in all-dielectric metasystems: fundamentals and applications. *Phys. Rep.* **1008**, 1–66 (2023).
6. Mie, G. Beiträge zur Optik trüber Medien, speziell kolloidaler Metallösungen. *Ann. Phys.* **330**, 377–445 (1908).
7. Feshbach, H. Unified theory of nuclear reactions. *Ann. Phys.* **5**, 357–390 (1958).
8. Feshbach, H. A unified theory of nuclear reactions. II. *Ann. Phys.* **19**, 287–313 (1962).
9. Liu, Z. et al. Locally resonant sonic materials. *Science* **289**, 1734–1736 (2000).
10. Liu, Z., Chan, C. T. & Sheng, P. Analytic model of phononic crystals with local resonances. *Phys. Rev. B* **71**, 14103 (2005).
11. Fang, N. et al. Ultrasonic metamaterials with negative modulus. *Nat. Mater.* **5**, 452–456 (2006).
12. Yang, Z., Mei, J., Yang, M., Chan, N. H. & Sheng, P. Membrane-type acoustic metamaterial with negative dynamic mass. *Phys. Rev. Lett.* **101**, 204301 (2008).
13. Yang, M., Ma, G., Yang, Z. & Sheng, P. Coupled membranes with doubly negative mass density and bulk modulus. *Phys. Rev. Lett.* **110**, 134301 (2013).
14. Wu, Y., Lai, Y. & Zhang, Z.-Q. Elastic metamaterials with simultaneously negative effective shear modulus and mass density. *Phys. Rev. Lett.* **107**, 105506 (2011).
15. Ding, Y., Liu, Z., Qiu, C. & Shi, J. Metamaterial with simultaneously negative bulk modulus and mass density. *Phys. Rev. Lett.* **99**, 93904 (2007).
16. Brunet, T. et al. Soft 3D acoustic metamaterial with negative index. *Nat. Mater.* **14**, 384–388 (2015).
17. Kaina, N., Lemoult, F., Fink, M. & Lerosey, G. Negative refractive index and acoustic superlens from multiple scattering in single negative metamaterials. *Nature* **525**, 77–81 (2015).
18. Li, J. & Chan, C. T. Double-negative acoustic metamaterial. *Phys. Rev. E* **70**, 55602 (2004).

19. Hsu, C. W., Zhen, B., Stone, A. D., Joannopoulos, J. D. & Soljačić, M. Bound states in the continuum. *Nat. Rev. Mater.* **1**, 16048 (2016).
20. Sadreev, A. F. Interference traps waves in an open system: bound states in the continuum. *Rep. Prog. Phys.* **84**, 55901 (2021).
21. El-Ganainy, R. et al. Non-Hermitian physics and PT symmetry. *Nat. Phys.* **14**, 11–19 (2018).
22. Miri, M.-A. & Alù, A. Exceptional points in optics and photonics. *Science* **363**, eaar7709 (2019).
23. Özdemir, Ş. K., Rotter, S., Nori, F. & Yang, L. Parity–time symmetry and exceptional points in photonics. *Nat. Mater.* **18**, 783–798 (2019).
24. Xue, H., Yang, Y. & Zhang, B. Topological acoustics. *Nat. Rev. Mater.* **7**, 974–990 (2022).
25. Kinsler, L. E., Frey, A., Coppens, A. B. & Sanders, J. V. *Fundamental of Acoustics* (Wiley, 2000).
26. Huang, L. et al. Sound trapping in an open resonator. *Nat. Commun.* **12**, 4819 (2021).
27. HEIN, S., KOCH, W. & NANNEN, L. Fano resonances in acoustics. *J. Fluid Mech.* **664**, 238–264 (2010).
28. Huang, S. et al. Acoustic perfect absorbers via Helmholtz resonators with embedded apertures. *J. Acoust. Soc. Am.* **145**, 254–262 (2019).
29. Zhu, X., Liang, B., Kan, W., Peng, Y. & Cheng, J. Deep-subwavelength-scale directional sensing based on highly localized dipolar Mie resonances. *Phys. Rev. Appl.* **5**, 54015 (2016).
30. Lu, G. et al. Realization of acoustic wave directivity at low frequencies with a subwavelength Mie resonant structure. *Appl. Phys. Lett.* **110**, 123507 (2017).
31. Zhao, J., Zhang, L. & Wu, Y. Enhancing monochromatic multipole emission by a subwavelength enclosure of degenerate Mie resonances. *J. Acoust. Soc. Am.* **142**, EL24–EL29 (2017).
32. Kuznetsov, A. I., Miroshnichenko, A. E., Brongersma, M. L., Kivshar, Y. S. & Luk'yanchuk, B. Optically resonant dielectric nanostructures. *Science* **354**, aag2472 (2016).
33. Kivshar, Y. & Miroshnichenko, A. Meta-optics with Mie resonances. *Opt. Photonics N.* **28**, 24 (2017).
34. Liang, Z. & Li, J. Extreme acoustic metamaterial by coiling up space. *Phys. Rev. Lett.* **108**, 114301 (2012).
35. Cheng, Y. et al. Ultra-sparse metasurface for high reflection of low-frequency sound based on artificial Mie resonances. *Nat. Mater.* **14**, 1013–1019 (2015).
36. Liang, Z. et al. Space-coiling metamaterials with double negativity and conical dispersion. *Sci. Rep.* **3**, 1614 (2013).
37. Xie, Y., Popa, B.-I., Zigoneanu, L. & Cummer, S. A. Measurement of a broadband negative index with space-coiling acoustic metamaterials. *Phys. Rev. Lett.* **110**, 175501 (2013).
38. Zhang, J., Cheng, Y. & Liu, X. Extraordinary acoustic transmission at low frequency by a tunable acoustic impedance metasurface based on coupled Mie resonators. *Appl. Phys. Lett.* **110**, 233502 (2017).
39. Zhou, C., Yuan, B., Cheng, Y. & Liu, X. Precise rainbow trapping for low-frequency acoustic waves with micro Mie resonance-based structures. *Appl. Phys. Lett.* **108**, 63501 (2016).
40. Li, Y. et al. Acoustic focusing by coiling up space. *Appl. Phys. Lett.* **101**, 233508 (2012).
41. Brunet, T., Leng, J. & Mondain-Monval, O. Soft acoustic metamaterials. *Science* **342**, 323–324 (2013).
42. Cai, Z. et al. Bubble architectures for locally resonant acoustic metamaterials. *Adv. Funct. Mater.* **29**, 1906984 (2019).
43. Boughzala, M., Stephan, O., Bossy, E., Dollet, B. & Marmottant, P. Polyhedral bubble vibrations. *Phys. Rev. Lett.* **126**, 54502 (2021).
44. Kafesaki, M., Penciu, R. S. & Economou, E. N. Air bubbles in water: a strongly multiple scattering medium for acoustic waves. *Phys. Rev. Lett.* **84**, 6050–6053 (2000).
45. Sharma, G. S., Skvortsov, A., MacGillivray, I. & Kessissoglou, N. Sound scattering by a bubble metasurface. *Phys. Rev. B* **102**, 214308 (2020).
46. Bok, E. et al. Metasurface for water-to-air sound transmission. *Phys. Rev. Lett.* **120**, 44302 (2018).
47. Bretagne, A., Tourin, A. & Leroy, V. Enhanced and reduced transmission of acoustic waves with bubble meta-screens. *Appl. Phys. Lett.* **99**, 221906 (2011).
48. Leroy, V. et al. Superabsorption of acoustic waves with bubble metascreens. *Phys. Rev. B* **91**, 20301 (2015).
49. Lanoy, M. et al. Subwavelength focusing in bubbly media using broadband time reversal. *Phys. Rev. B* **91**, 224202 (2015).
50. Huang, T.-Y., Shen, C. & Jing, Y. Membrane- and plate-type acoustic metamaterials. *J. Acoust. Soc. Am.* **139**, 3240–3250 (2016).
51. Jenkins, C. H. M. & Korde, U. A. Membrane vibration experiments: an historical review and recent results. *J. Sound. Vib.* **295**, 602–613 (2006).
52. Ma, G., Yang, M., Xiao, S., Yang, Z. & Sheng, P. Acoustic metasurface with hybrid resonances. *Nat. Mater.* **13**, 873–878 (2014).
53. Ebbesen, T. W., Lezec, H. J., Ghaemi, H. F., Thio, T. & Wolff, P. A. Extraordinary optical transmission through sub-wavelength hole arrays. *Nature* **391**, 667–669 (1998).
54. Lu, M.-H. et al. Extraordinary acoustic transmission through a 1D grating with very narrow apertures. *Phys. Rev. Lett.* **99**, 174301 (2007).
55. Hou, B. et al. Tuning Fabry–Perot resonances via diffraction evanescent waves. *Phys. Rev. B* **76**, 54303 (2007).
56. Christensen, J., Martin-Moreno, L. & Garcia-Vidal, F. J. Theory of resonant acoustic transmission through subwavelength apertures. *Phys. Rev. Lett.* **101**, 14301 (2008).
57. Zhu, J. et al. A holey-structured metamaterial for acoustic deep-subwavelength imaging. *Nat. Phys.* **7**, 52–55 (2011).
58. Yang, M. & Sheng, P. Sound absorption structures: from porous media to acoustic metamaterials. *Annu. Rev. Mater. Res.* **47**, 83–114 (2017).
59. Stinson, M. R. The propagation of plane sound waves in narrow and wide circular tubes, and generalization to uniform tubes of arbitrary cross-sectional shape. *J. Acoust. Soc. Am.* **89**, 550–558 (1991).
60. Qu, S. & Sheng, P. Microwave and acoustic absorption metamaterials. *Phys. Rev. Appl.* **17**, 47001 (2022).
61. Yang, M. & Sheng, P. Acoustic metamaterial absorbers: the path to commercialization. *Appl. Phys. Lett.* **122**, 260504 (2023).
62. Huang, S., Li, Y., Zhu, J. & Tsai, D. P. Sound-absorbing materials. *Phys. Rev. Appl.* **20**, 10501 (2023).
63. Fan, S., Suh, W. & Joannopoulos, J. D. Temporal coupled-mode theory for the Fano resonance in optical resonators. *J. Opt. Soc. Am. A* **20**, 569–572 (2003).
64. Xu, Y., Li, Y., Lee, R. K. & Yariv, A. Scattering-theory analysis of waveguide–resonator coupling. *Phys. Rev. E* **62**, 7389–7404 (2000).
65. Gu, Z. et al. Controlling sound in non-Hermitian acoustic systems. *Phys. Rev. Appl.* **16**, 57001 (2021).
66. Bliokh, K. Y., Bliokh, Y. P., Freilikher, V., Savel'ev, S. & Nori, F. Colloquium: unusual resonators: plasmonics, metamaterials, and random media. *Rev. Mod. Phys.* **80**, 1201–1213 (2008).
67. Jiménez, N., Huang, W., Romero-García, V., Pagneux, V. & Groby, J.-P. Ultra-thin metamaterial for perfect and quasi-omnidirectional sound absorption. *Appl. Phys. Lett.* **109**, 121902 (2016).
68. Romero-García, V., Theocharis, G., Richoux, O. & Pagneux, V. Use of complex frequency plane to design broadband and sub-wavelength absorbers. *J. Acoust. Soc. Am.* **139**, 3395–3403 (2016).
69. Romero-García, V. et al. Perfect and broadband acoustic absorption by critically coupled sub-wavelength resonators. *Sci. Rep.* **6**, 19519 (2016).
70. Long, H., Cheng, Y., Tao, J. & Liu, X. Perfect absorption of low-frequency sound waves by critically coupled subwavelength resonant system. *Appl. Phys. Lett.* **110**, 23502 (2017).
71. Yang, M. et al. Subwavelength total acoustic absorption with degenerate resonators. *Appl. Phys. Lett.* **107**, 104104 (2015).
72. Aurégan, Y. Ultra-thin low frequency perfect sound absorber with high ratio of active area. *Appl. Phys. Lett.* **113**, 201904 (2018).
73. Cai, X., Guo, Q., Hu, G. & Yang, J. Ultrathin low-frequency sound absorbing panels based on coplanar spiral tubes or coplanar Helmholtz resonators. *Appl. Phys. Lett.* **105**, 121901 (2014).
74. Liu, L., Chang, H., Zhang, C. & Hu, X. Single-channel labyrinthine metasurfaces as perfect sound absorbers with tunable bandwidth. *Appl. Phys. Lett.* **111**, 83503 (2017).
75. Huang, S. et al. Acoustic perfect absorbers via spiral metasurfaces with embedded apertures. *Appl. Phys. Lett.* **113**, 233501 (2018).
76. Wang, Y. et al. A tunable sound-absorbing metamaterial based on coiled-up space. *J. Appl. Phys.* **123**, 185109 (2018).
77. Donda, K. et al. Extreme low-frequency ultrathin acoustic absorbing metasurface. *Appl. Phys. Lett.* **115**, 173506 (2019).
78. Li, D. T., Huang, S. B., Cheng, Y. & Li, Y. Compact asymmetric sound absorber at the exceptional point. *Sci. China Phys., Mech. Astron.* **64**, 244303 (2021).
79. Guo, J., Zhang, X., Fang, Y. & Qu, R. An extremely-thin acoustic metasurface for low-frequency sound attenuation with a tunable absorption bandwidth. *Int. J. Mech. Sci.* **213**, 106872 (2022).
80. Li, Y. & Assouar, B. M. Acoustic metasurface-based perfect absorber with deep subwavelength thickness. *Appl. Phys. Lett.* **108**, 63502 (2016).
81. Zhang, C. & Hu, X. Three-dimensional single-port labyrinthine acoustic metamaterial: perfect absorption with large bandwidth and tunability. *Phys. Rev. Appl.* **6**, 64025 (2016).
82. Long, H., Shao, C., Liu, C., Cheng, Y. & Liu, X. Broadband near-perfect absorption of low-frequency sound by subwavelength metasurface. *Appl. Phys. Lett.* **115**, 103503 (2019).
83. Li, J., Wang, W., Xie, Y., Popa, B.-I. & Cummer, S. A. A sound absorbing metasurface with coupled resonators. *Appl. Phys. Lett.* **109**, 91908 (2016).
84. Yang, M., Chen, S., Fu, C. & Sheng, P. Optimal sound-absorbing structures. *Mater. Horiz.* **4**, 673–680 (2017).
85. Zhu, Y., Donda, K., Fan, S., Cao, L. & Assouar, B. Broadband ultra-thin acoustic metasurface absorber with coiled structure. *Appl. Phys. Express* **12**, 114002 (2019).
86. Gao, N., Luo, D., Cheng, B. & Hou, H. Teaching-learning-based optimization of a composite metastructure in the 0–10 kHz broadband sound absorption range. *J. Acoust. Soc. Am.* **148**, EL125–EL129 (2020).
87. Jiménez, N., Romero-García, V., Pagneux, V. & Groby, J.-P. Rainbow-trapping absorbers: broadband, perfect and asymmetric sound absorption by subwavelength panels for transmission problems. *Sci. Rep.* **7**, 13595 (2017).
88. Peng, X., Ji, J. & Jing, Y. Composite honeycomb metasurface panel for broadband sound absorption. *J. Acoust. Soc. Am.* **144**, EL255–EL261 (2018).
89. Liu, C. R., Wu, J. H., Ma, F., Chen, X. & Yang, Z. A thin multi-order Helmholtz metamaterial with perfect broadband acoustic absorption. *Appl. Phys. Express* **12**, 84002 (2019).
90. Long, H. et al. Tunable and broadband asymmetric sound absorptions with coupling of acoustic bright and dark modes. *J. Sound. Vib.* **479**, 115371 (2020).
91. Rui Liu, C., Hui, Wu,J., Yang, Z. & Ma, F. Ultra-broadband acoustic absorption of a thin microperforated panel metamaterial with multi-order resonance. *Compos. Struct.* **246**, 112366 (2020).
92. Long, H., Gao, S., Cheng, Y. & Liu, X. Multiband quasi-perfect low-frequency sound absorber based on double-channel Mie resonator. *Appl. Phys. Lett.* **112**, 33507 (2018).

93. Yu, Z., Raman, A. & Fan, S. Fundamental limit of nanophotonic light trapping in solar cells. *Proc. Natl Acad. Sci. USA* **107**, 17491 LP–17417496 (2010).
94. Zhou, Z., Huang, S., Li, D., Zhu, J. & Li, Y. Broadband impedance modulation via non-local acoustic metamaterials. *Natl Sci. Rev.* **9**, nwab171 (2022).
95. Huang, S. et al. Compact broadband acoustic sink with coherently coupled weak resonances. *Sci. Bull.* **65**, 373–379 (2020).
96. Huang, S. et al. Broadband sound attenuation by metaliner under grazing flow. *Appl. Phys. Lett.* **118**, 63504 (2021).
97. Rajendran, V., Piacsek, A. & Méndez Echenagucia, T. Design of broadband Helmholtz resonator arrays using the radiation impedance method. *J. Acoust. Soc. Am.* **151**, 457–466 (2022).
98. Zhu, Y. et al. Nonlocal acoustic metasurface for ultrabroadband sound absorption. *Phys. Rev. B* **103**, 64102 (2021).
99. Li, X., Yu, X. & Zhai, W. Additively manufactured deformation-recoverable and broadband sound-absorbing microlattice inspired by the concept of traditional perforated panels. *Adv. Mater.* **33**, 2104552 (2021).
100. Dong, R., Mao, D., Wang, X. & Li, Y. Ultrabroadband acoustic ventilation barriers via hybrid-functional metasurfaces. *Phys. Rev. Appl.* **15**, 24044 (2021).
101. Ren, Z., Cheng, Y., Chen, M., Yuan, X. & Fang, D. A compact multifunctional metastructure for low-frequency broadband sound absorption and crash energy dissipation. *Mater. Des.* **215**, 110462 (2022).
102. Chen, A. et al. Machine learning-assisted low-frequency and broadband sound absorber with coherently coupled weak resonances. *Appl. Phys. Lett.* **120**, 33501 (2022).
103. Liu, L. et al. Broadband acoustic absorbing metamaterial via deep learning approach. *Appl. Phys. Lett.* **120**, 251701 (2022).
104. Ding, H. et al. Broadband acoustic meta-liner with metal foam approaching causality-governed minimal thickness. *Int. J. Mech. Sci.* **232**, 107601 (2022).
105. Shao, C. et al. Metasurface absorber for ultra-broadband sound via over-damped modes coupling. *Appl. Phys. Lett.* **120**, 83504 (2022).
106. Wang, N. et al. Meta-silencer with designable timbre. *Int. J. Extrem. Manuf.* **5**, 25501 (2023).
107. Jiang, X., Li, Y., Liang, B., Cheng, J. & Zhang, L. Convert acoustic resonances to orbital angular momentum. *Phys. Rev. Lett.* **117**, 34301 (2016).
108. Jiang, X., Liang, B., Cheng, J.-C. & Qiu, C.-W. Twisted acoustics: metasurface-enabled multiplexing and demultiplexing. *Adv. Mater.* **30**, 1800257 (2018).
109. Fu, Y. et al. Sound vortex diffraction via topological charge in phase gradient metagratings. *Sci. Adv.* **6**, eaba9876 (2023).
110. Zou, Z., Lirette, R. & Zhang, L. Orbital angular momentum reversal and asymmetry in acoustic vortex beam reflection. *Phys. Rev. Lett.* **125**, 74301 (2020).
111. Chen, H. Z. et al. Revealing the missing dimension at an exceptional point. *Nat. Phys.* **16**, 571–578 (2020).
112. Wang, Q. et al. Acoustic topological beam nonreciprocity via the rotational Doppler effect. *Sci. Adv.* **8**, eabq4451 (2023).
113. Fu, Y. et al. Asymmetric generation of acoustic vortex using dual-layer metasurfaces. *Phys. Rev. Lett.* **128**, 104501 (2022).
114. Volke-Sepúlveda, K., Santillán, A. O. & Boullosa, R. R. Transfer of angular momentum to matter from acoustical vortices in free space. *Phys. Rev. Lett.* **100**, 24302 (2008).
115. Anhäuser, A., Wunenburger, R. & Brasselet, E. Acoustic rotational manipulation using orbital angular momentum transfer. *Phys. Rev. Lett.* **109**, 34301 (2012).
116. Courtney, C. R. P. et al. Independent trapping and manipulation of microparticles using dexterous acoustic tweezers. *Appl. Phys. Lett.* **104**, 154103 (2014).
117. Shi, C., Dubois, M., Wang, Y. & Zhang, X. High-speed acoustic communication by multiplexing orbital angular momentum. *Proc. Natl Acad. Sci. USA* **114**, 7250–7253 (2017).
118. Liu, C. et al. Broadband acoustic vortex beam generator based on coupled resonances. *Appl. Phys. Lett.* **118**, 143503 (2021).
119. Li, J., Fok, L., Yin, X., Bartal, G. & Zhang, X. Experimental demonstration of an acoustic magnifying hyperlens. *Nat. Mater.* **8**, 931–934 (2009).
120. Lemoult, F., Fink, M. & Lerosey, G. Acoustic resonators for far-field control of sound on a subwavelength scale. *Phys. Rev. Lett.* **107**, 64301 (2011).
121. Molerón, M. & Daraio, C. Acoustic metamaterial for subwavelength edge detection. *Nat. Commun.* **6**, 8037 (2015).
122. Zhu, Y. et al. Fine manipulation of sound via lossy metamaterials with independent and arbitrary reflection amplitude and phase. *Nat. Commun.* **9**, 1632 (2018).
123. Tian, Z. et al. Programmable acoustic metasurfaces. *Adv. Funct. Mater.* **29**, 1808489 (2019).
124. Liu, T., Chen, F., Liang, S., Gao, H. & Zhu, J. Subwavelength sound focusing and imaging via gradient metasurface-enabled spoof surface acoustic wave modulation. *Phys. Rev. Appl.* **11**, 34061 (2019).
125. Tian, Y. et al. Far-field subwavelength acoustic computational imaging with a single detector. *Phys. Rev. Appl.* **18**, 14046 (2022).
126. Landi, M., Zhao, J., Prather, W. E., Wu, Y. & Zhang, L. Acoustic Purcell effect for enhanced emission. *Phys. Rev. Lett.* **120**, 114301 (2018).
127. Schmidt, M. K., Helt, L. G., Poulton, C. G. & Steel, M. J. Elastic Purcell effect. *Phys. Rev. Lett.* **121**, 64301 (2018).
128. Song, Y. et al. Strong collimated emission enhancement by acoustic metasurfaces. *Phys. Rev. Appl.* **12**, 54012 (2019).
129. Huang, S. et al. Acoustic Purcell effect induced by quasibound state in the continuum. *Fundam. Res.* https://doi.org/10.1016/j.fmre.2022.06.009 (2022).
130. Lyapina, A. A., Maksimov, D. N., Pilipchuk, A. S. & Sadreev, A. F. Bound states in the continuum in open acoustic resonators. *J. Fluid Mech.* **780**, 370–387 (2015).
131. Deriy, I., Toftul, I., Petrov, M. & Bogdanov, A. Bound states in the continuum in compact acoustic resonators. *Phys. Rev. Lett.* **128**, 84301 (2022).
132. Parker, R. Resonance effects in wake shedding from parallel plates: calculation of resonant frequencies. *J. Sound. Vib.* **5**, 330–343 (1967).
133. Hein, S. & Koch, W. Acoustic resonances and trapped modes in pipes and tunnels. *J. Fluid Mech.* **605**, 401–428 (2008).
134. Linton, C. M., McIver, M., McIver, P., Ratcliffe, K. & Zhang, J. Trapped modes for off-centre structures in guides. *Wave Motion* **36**, 67–85 (2002).
135. Duan, Y., Koch, W., Linton, C. M. & McIver, M. Complex resonances and trapped modes in ducted domains. *J. Fluid Mech.* **571**, 119–147 (2007).
136. Evans, D. & Porter, R. Trapped modes embedded in the continuous spectrum. *Q. J. Mech. Appl. Math.* **51**, 263–274 (1998).
137. Jacobsen, R. E., Krasnok, A., Arslanagić, S., Lavrinenko, A. V. & Alú, A. Boundary-induced embedded eigenstate in a single resonator for advanced sensing. *ACS Photonics* **9**, 1936–1943 (2022).
138. Linton, C. & McIver, M. Trapped modes in cylindrical waveguides. *Q. J. Mech. Appl. Math.* **51**, 389–412 (1998).
139. Linton, C. M. & McIver, P. Embedded trapped modes in water waves and acoustics. *Wave Motion* **45**, 16–29 (2007).
140. Rotter, I. A continuum shell model for the open quantum mechanical nuclear system. *Rep. Prog. Phys.* **54**, 635 (1991).
141. Okołowicz, J., Płoszajczak, M. & Rotter, I. Dynamics of quantum systems embedded in a continuum. *Phys. Rep.* **374**, 271–383 (2003).
142. Dittes, F.-M. The decay of quantum systems with a small number of open channels. *Phys. Rep.* **339**, 215–316 (2000).
143. Sadreev, A. F. & Rotter, I. S-matrix theory for transmission through billiards in tight-binding approach. *J. Phys. A. Math. Gen.* **36**, 11413–11433 (2003).
144. Maksimov, D. N., Sadreev, A. F., Lyapina, A. A. & Pilipchuk, A. S. Coupled mode theory for acoustic resonators. *Wave Motion* **56**, 52–66 (2015).
145. Pichugin, K., Schanz, H. & Šeba, P. Effective coupling for open billiards. *Phys. Rev. E* **64**, 56227 (2001).
146. Parker, R. Resonance effects in wake shedding from parallel plates: some experimental observations. *J. Sound. Vib.* **4**, 62–72 (1966).
147. Huang, S. et al. Extreme sound confinement from quasibound states in the continuum. *Phys. Rev. Appl.* **14**, 21001 (2020).
148. Jia, B. et al. Bound states in the continuum protected by reduced symmetry of three-dimensional open acoustic resonators. *Phys. Rev. Appl.* **19**, 54001 (2023).
149. Hsu, C. W. et al. Observation of trapped light within the radiation continuum. *Nature* **499**, 188–191 (2013).
150. Huang, L. et al. General framework of bound states in the continuum in an open acoustic resonator. *Phys. Rev. Appl.* **18**, 54021 (2022).
151. Pilipchuk, A. S. & Sadreev, A. F. Accidental bound states in the continuum in an open Sinai billiard. *Phys. Lett. A* **381**, 720–724 (2017).
152. Lyapina, A. A., Pilipchuk, A. S. & Sadreev, A. F. Trapped modes in a non-axisymmetric cylindrical waveguide. *J. Sound. Vib.* **421**, 48–60 (2018).
153. Friedrich, H. & Wintgen, D. Interfering resonances and bound states in the continuum. *Phys. Rev. A* **32**, 3231–3242 (1985).
154. Suh, W., Wang, Z. & Fan, S. Temporal coupled-mode theory and the presence of non-orthogonal modes in lossless multimode cavities. *IEEE J. Quantum Electron.* **40**, 1511–1518 (2004).
155. Volya, A. & Zelevinsky, V. Non-Hermitian effective Hamiltonian and continuum shell model. *Phys. Rev. C.* **67**, 54322 (2003).
156. Pilipchuk, A. S., Pilipchuk, A. A. & Sadreev, A. F. Bound states in the continuum in open spherical resonator. *Phys. Scr.* **95**, 85002 (2020).
157. Sadreev, A. F., Bulgakov, E. N. & Rotter, I. Bound states in the continuum in open quantum billiards with a variable shape. *Phys. Rev. B* **73**, 235342 (2006).
158. Huang, L., Xu, L., Rahmani, M., Neshev, D. & Miroshnichenko, A. E. Pushing the limit of high-Q mode of a single dielectric nanocavity. *Adv. Photonics* **3**, 016004 (2021).
159. Rybin, M. V. et al. High-Q supercavity modes in subwavelength dielectric resonators. *Phys. Rev. Lett.* **119**, 243901(2017).
160. Fan, S. et al. Theoretical analysis of channel drop tunneling processes. *Phys. Rev. B* **59**, 15882–15892 (1999).
161. Bulgakov, E. N. & Sadreev, A. F. Bound states in the continuum in photonic waveguides inspired by defects. *Phys. Rev. B* **78**, 75105 (2008).
162. Hein, S., Koch, W. & Nannen, L. Trapped modes and Fano resonances in two-dimensional acoustical duct–cavity systems. *J. Fluid Mech.* **692**, 257–287 (2012).
163. Sadreev, A. F., Bulgakov, E. N. & Rotter, I. Trapping of an electron in the transmission through two quantum dots coupled by a wire. *J. Exp. Theor. Phys. Lett.* **82**, 498–503 (2005).
164. Huang, L. et al. Topological supercavity resonances in the finite system. *Adv. Sci.* https://doi.org/10.1002/advs.202200257 (2022).
165. Bulgakov, E. N. & Maksimov, D. N. Bound states in the continuum and polarization singularities in periodic arrays of dielectric rods. *Phys. Rev. A* **96**, 63833 (2017).
166. Jin, J. et al. Topologically enabled ultrahigh-Q guided resonances robust to out-of-plane scattering. *Nature* **574**, 501–504 (2019).
167. Cao, L. et al. Perfect absorption of flexural waves induced by bound state in the continuum. *Extrem. Mech. Lett.* **47**, 101364 (2021).

168. Cao, L. et al. Elastic bound state in the continuum with perfect mode conversion. *J. Mech. Phys. Solids* **154**, 104502 (2021).
169. Zhou, Z., Jia, B., Wang, N., Wang, X. & Li, Y. Observation of perfectly-chiral exceptional point via bound state in the continuum. *Phys. Rev. Lett.* **130**, 116101 (2023).
170. Srivastava, A. Causality and passivity in elastodynamics. *Proc. R. Soc. A* **471**, 20150256 (2015).
171. Muhlestein, M. B., Sieck, C. F., Alù, A. & Haberman, M. R. Reciprocity, passivity and causality in Willis materials. *Proc. R. Soc. A* **472**, 20160604 (2016).
172. Mangulis, V. Kramers–Kronig or dispersion relations in acoustics. *J. Acoust. Soc. Am.* **36**, 211–212 (1964).
173. Gao, N. et al. Acoustic metamaterials for noise reduction: a review. *Adv. Mater. Technol.* **7**, 2100698 (2022).
174. Zangeneh-Nejad, F. & Fleury, R. Active times for acoustic metamaterials. *Rev. Phys.* **4**, 100031 (2019).
175. Ji, G. & Huber, J. Recent progress in acoustic metamaterials and active piezoelectric acoustic metamaterials — a review. *Appl. Mater. Today* **26**, 101260 (2022).
176. Willatzen, M. & Christensen, J. Acoustic gain in piezoelectric semiconductors at ε-near-zero response. *Phys. Rev. B* **89**, 041201 (2014).
177. Hutson, A. R., McFee, J. H. & White, D. L. Ultrasonic amplification in CdS. *Phys. Rev. Lett.* **7**, 237–239 (1961).
178. Trainiti, G. et al. Time-periodic stiffness modulation in elastic metamaterials for selective wave filtering: theory and experiment. *Phys. Rev. Lett.* **122**, 124301 (2019).
179. Bergamini, A. et al. Phononic crystal with adaptive connectivity. *Adv. Mater.* **26**, 1343–1347 (2014).
180. Ma, G., Fan, X., Sheng, P. & Fink, M. Shaping reverberating sound fields with an actively tunable metasurface. *Proc. Natl Acad. Sci. USA* **115**, 6638–6643 (2018).
181. Chen, Y. et al. Nonreciprocal wave propagation in a continuum-based metamaterial with space-time modulated resonators. *Phys. Rev. Appl.* **11**, 64052 (2019).
182. Wang, Z., Zhang, Q., Zhang, K. & Hu, G. Tunable digital metamaterial for broadband vibration isolation at low frequency. *Adv. Mater.* **28**, 9857–9861 (2016).
183. Bilal, O. R., Foehr, A. & Daraio, C. Reprogrammable phononic metasurfaces. *Adv. Mater.* **29**, 1700628 (2017).
184. Fleury, R., Sounas, D. L., Sieck, C. F., Haberman, M. R. & Alù, A. Sound isolation and giant linear nonreciprocity in a compact acoustic circulator. *Science* **343**, 516–519 (2014).
185. Quan, L., Yves, S., Peng, Y., Esfahlani, H. & Alù, A. Odd Willis coupling induced by broken time-reversal symmetry. *Nat. Commun.* **12**, 2615 (2021).
186. Wang, P., Lu, L. & Bertoldi, K. Topological phononic crystals with one-way elastic edge waves. *Phys. Rev. Lett.* **115**, 104302 (2015).
187. Shen, C., Zhu, X., Li, J. & Cummer, S. A. Nonreciprocal acoustic transmission in space-time modulated coupled resonators. *Phys. Rev. B* **100**, 54302 (2019).
188. Fleury, R., Sounas, D. & Alù, A. An invisible acoustic sensor based on parity–time symmetry. *Nat. Commun.* **6**, 5905 (2015).
189. Rasmussen, C. & Alù, A. Non-Foster acoustic radiation from an active piezoelectric transducer. *Proc. Natl Acad. Sci. USA* **118**, e2024984118 (2021).
190. Chen, Z. et al. Efficient nonreciprocal mode transitions in spatiotemporally modulated acoustic metamaterials. *Sci. Adv.* **7**, eabj1198 (2023).
191. Cho, C., Wen, X., Park, N. & Li, J. Digitally virtualized atoms for acoustic metamaterials. *Nat. Commun.* **11**, 251 (2020).
192. Wen, X. et al. Unidirectional amplification with acoustic non-Hermitian space–time varying metamaterial. *Commun. Phys.* **5**, 18 (2022).
193. Popa, B.-I., Zhai, Y. & Kwon, H.-S. Broadband sound barriers with bianisotropic metasurfaces. *Nat. Commun.* **9**, 5299 (2018).
194. Brandenbourger, M., Locsin, X., Lerner, E. & Coulais, C. Non-reciprocal robotic metamaterials. *Nat. Commun.* **10**, 4608 (2019).
195. Rupin, M., Lerosey, G., de Rosny, J. & Lemoult, F. Mimicking the cochlea with an active acoustic metamaterial. *N. J. Phys.* **21**, 93012 (2019).
196. Koutserimpas, T. T., Rivet, E., Lissek, H. & Fleury, R. Active acoustic resonators with reconfigurable resonance frequency, absorption, and bandwidth. *Phys. Rev. Appl.* **12**, 54064 (2019).
197. Sirota, L., Ilan, R., Shokef, Y. & Lahini, Y. Non-newtonian topological mechanical metamaterials using feedback control. *Phys. Rev. Lett.* **125**, 256802 (2020).
198. Souslov, A., van Zuiden, B. C., Bartolo, D. & Vitelli, V. Topological sound in active-liquid metamaterials. *Nat. Phys.* **13**, 1091–1094 (2017).
199. Shankar, S., Souslov, A., Bowick, M. J., Marchetti, M. C. & Vitelli, V. Topological active matter. *Nat. Rev. Phys.* **4**, 380–398 (2022).
200. Aliev, A. E., Lima, M. D., Fang, S. & Baughman, R. H. Underwater sound generation using carbon nanotube projectors. *Nano Lett.* **10**, 2374–2380 (2010).
201. Xiao, L. et al. Flexible, stretchable, transparent carbon nanotube thin film loudspeakers. *Nano Lett.* **8**, 4539–4545 (2008).
202. Pierce, C. D. et al. Adaptive elastic metastructures from magneto-active elastomers. *Smart Mater. Struct.* **29**, 65004 (2020).
203. Xu, Z. et al. Vat photopolymerization of fly-like, complex micro-architectures with dissolvable supports. *Addit. Manuf.* **47**, 102321 (2021).
204. Gliozzi, A. S. et al. Tunable photo-responsive elastic metamaterials. *Nat. Commun.* **11**, 2576 (2020).
205. Sergeev, S. et al. Development of a plasma electroacoustic actuator for active noise control applications. *J. Phys. D* **53**, 495202 (2020).
206. Cha, J. & Daraio, C. Electrical tuning of elastic wave propagation in nanomechanical lattices at MHz frequencies. *Nat. Nanotechnol.* **13**, 1016–1020 (2018).
207. Shao, L. et al. Electrical control of surface acoustic waves. *Nat. Electron.* **5**, 348–355 (2022).
208. Chu, Y. et al. Quantum acoustics with superconducting qubits. *Science* **358**, 199–202 (2017).
209. del Pino, J., Slim, J. J. & Verhagen, E. Non-Hermitian chiral phononics through optomechanically induced squeezing. *Nature* **606**, 82–87 (2022).
210. Popa, B.-I., Shinde, D., Konneker, A. & Cummer, S. A. Active acoustic metamaterials reconfigurable in real time. *Phys. Rev. B* **91**, 220303 (2015).
211. Wang, Q., del Hougne, P. & Ma, G. Controlling the spatiotemporal response of transient reverberating sound. *Phys. Rev. Appl.* **17**, 44007 (2022).
212. Nassar, H. et al. Nonreciprocity in acoustic and elastic materials. *Nat. Rev. Mater.* **5**, 667–685 (2020).
213. Zhu, Y. et al. Janus acoustic metascreen with nonreciprocal and reconfigurable phase modulations. *Nat. Commun.* **12**, 7089 (2021).
214. Fleury, R., Sounas, D. L. & Alù, A. Subwavelength ultrasonic circulator based on spatiotemporal modulation. *Phys. Rev. B* **91**, 174306 (2015).
215. Zhu, X. et al. Tunable unidirectional compact acoustic amplifier via space-time modulated membranes. *Phys. Rev. B* **102**, 24309 (2020).
216. Popa, B.-I. & Cummer, S. A. Non-reciprocal and highly nonlinear active acoustic metamaterials. *Nat. Commun.* **5**, 3398 (2014).
217. Gu, Z., Hu, J., Liang, B., Zou, X. & Cheng, J. Broadband non-reciprocal transmission of sound with invariant frequency. *Sci. Rep.* **6**, 19824 (2016).
218. Chen, Y., Li, X., Scheibner, C., Vitelli, V. & Huang, G. Realization of active metamaterials with odd micropolar elasticity. *Nat. Commun.* **12**, 5935 (2021).
219. Scheibner, C. et al. Odd elasticity. *Nat. Phys.* **16**, 475–480 (2020).
220. Li, H., Mekawy, A., Krasnok, A. & Alù, A. Virtual parity-time symmetry. *Phys. Rev. Lett.* **124**, 193901 (2020).
221. Ra'di, Y., Krasnok, A. & Alù, A. Virtual critical coupling. *ACS Photonics* **7**, 1468–1475 (2020).
222. Trainiti, G., Ra'di, Y., Ruzzene, M. & Alù, A. Coherent virtual absorption of elastodynamic waves. *Sci. Adv.* **5**, eaaw3255 (2023).
223. Bender, C. M. Making sense of non-Hermitian hamiltonians. *Rep. Prog. Phys.* **70**, 947–1018 (2007).
224. Bender, C. M. & Boettcher, S. Real spectra in non-Hermitian Hamiltonians having PT symmetry. *Phys. Rev. Lett.* **80**, 5243–5246 (1998).
225. Bender, C. M., Brody, D. C. & Jones, H. F. Complex extension of quantum mechanics. *Phys. Rev. Lett.* **89**, 270401 (2002).
226. Mostafazadeh, A. Spectral singularities of complex scattering potentials and infinite reflection and transmission coefficients at real energies. *Phys. Rev. Lett.* **102**, 220402 (2009).
227. Zhu, X., Ramezani, H., Shi, C., Zhu, J. & Zhang, X. PT-symmetric acoustics. *Phys. Rev. X* **4**, 031042 (2014).
228. Christensen, J., Willatzen, M., Velasco, V. R. & Lu, M.-H. Parity–time synthetic phononic media. *Phys. Rev. Lett.* **116**, 207601 (2016).
229. Shi, C. et al. Accessing the exceptional points of parity-time symmetric acoustics. *Nat. Commun.* **7**, 11110 (2016).
230. Fleury, R., Sounas, D. L. & Alù, A. Parity-time symmetry in acoustics: theory, devices, and potential applications. *IEEE J. Sel. Top. Quantum Electron.* **22**, 5000809 (2016).
231. Magariyachi, T., Arias Casals, H., Herrero, R., Botey, M. & Staliunas, K. PT-symmetric Helmholtz resonator dipoles for sound directivity. *Phys. Rev. B* **103**, 94201 (2021).
232. Li, H. et al. Ultrathin acoustic parity-time symmetric metasurface cloak. *Research* **2019**, 8345683 (2019).
233. Yang, W. J., Yang, Z. Z., Guan, A. Y., Zou, X. Y. & Cheng, J. C. Design and experimental demonstration of effective acoustic gain medium for PT-symmetric refractive index. *Appl. Phys. Lett.* **120**, 063503 (2022).
234. Merkel, A., Romero-García, V., Groby, J. P., Li, J. & Christensen, J. Unidirectional zero sonic reflection in passive PT-symmetric Willis media. *Phys. Rev. B* **98**, 201102(R) (2018).
235. Shen, C., Li, J., Peng, X. & Cummer, S. A. Synthetic exceptional points and unidirectional zero reflection in non-Hermitian acoustic systems. *Phys. Rev. Mater.* **2**, 125203 (2018).
236. Liu, Y. et al. Willis metamaterial on a structured beam. *Phys. Rev. X* **9**, 011040 (2019).
237. Liu, T., Zhu, X., Chen, F., Liang, S. & Zhu, J. Unidirectional wave vector manipulation in two-dimensional space with an all passive acoustic parity-time-symmetric metamaterials crystal. *Phys. Rev. Lett.* **120**, 124502 (2018).
238. Stojanoska, K. & Shen, C. Non-Hermitian planar elastic metasurface for unidirectional focusing of flexural waves. *Appl. Phys. Lett.* **120**, 241701 (2022).
239. Wang, X., Fang, X., Mao, D., Jing, Y. & Li, Y. Extremely asymmetrical acoustic metasurface mirror at the exceptional point. *Phys. Rev. Lett.* **123**, 214302 (2019).
240. Yang, Y., Jia, H., Bi, Y., Zhao, H. & Yang, J. Experimental demonstration of an acoustic asymmetric diffraction grating based on passive parity-time-symmetric medium. *Phys. Rev. Appl.* **12**, 034040 (2019).
241. Liu, T. et al. Single-sided acoustic beam splitting based on parity-time symmetry. *Phys. Rev. B* **102**, 014306 (2020).
242. Fang, X. et al. Observation of higher-order exceptional points in a non-local acoustic metagrating. *Commun. Phys.* **4**, 271 (2021).
243. Zhang, J. et al. Giant nonlinearity via breaking parity-time symmetry: a route to low-threshold phonon diodes. *Phys. Rev. B* **92**, 115407 (2015).
244. Shao, L. et al. Non-reciprocal transmission of microwave acoustic waves in nonlinear parity–time symmetric resonators. *Nat. Electron.* **3**, 267–272 (2020).
245. Ding, K., Ma, G., Xiao, M., Zhang, Z. Q. & Chan, C. T. Emergence, coalescence, and topological properties of multiple exceptional points and their experimental realization. *Phys. Rev. X* **6**, 021007 (2016).

246. Ding, K., Ma, G., Zhang, Z. Q. & Chan, C. T. Experimental demonstration of an anisotropic exceptional point. *Phys. Rev. Lett.* **121**, 85702 (2018).
247. Achilleos, V., Theocharis, G., Richoux, O. & Pagneux, V. Non-Hermitian acoustic metamaterials: role of exceptional points in sound absorption. *Phys. Rev. B* **95**, 144303 (2017).
248. Lee, T., Nomura, T., Dede, E. M. & Iizuka, H. Asymmetric loss-induced perfect sound absorption in duct silencers. *Appl. Phys. Lett.* **116**, 214101 (2020).
249. Liu, T. et al. Chirality-switchable acoustic vortex emission via non-Hermitian selective excitation at an exceptional point. *Sci. Bull.* **67**, 1131–1136 (2022).
250. Tang, W. et al. Exceptional nexus with a hybrid topological invariant. *Science* **370**, 1077–1080 (2020).
251. Tang, W., Ding, K. & Ma, G. Direct measurement of topological properties of an exceptional parabola. *Phys. Rev. Lett.* **127**, 34301 (2021).
252. Mensah, G. A., Magri, L., Silva, C. F., Buschmann, P. E. & Moeck, J. P. Exceptional points in the thermoacoustic spectrum. *J. Sound. Vib.* **433**, 124–128 (2018).
253. Bourquard, C. & Noiray, N. Stabilization of acoustic modes using Helmholtz and quarter-wave resonators tuned at exceptional points. *J. Sound. Vib.* **445**, 288–307 (2019).
254. Liu, J. J. et al. Experimental realization of weyl exceptional rings in a synthetic three-dimensional non-Hermitian phononic crystal. *Phys. Rev. Lett.* **129**, 084301 (2022).
255. Zhang, Q. et al. Observation of acoustic non-Hermitian Bloch braids and associated topological phase transitions. *Phys. Rev. Lett.* **130**, 17201 (2023).
256. Guo, C.-X., Chen, S., Ding, K. & Hu, H. Exceptional non-Abelian topology in multiband non-Hermitian systems. *Phys. Rev. Lett.* **130**, 157201 (2023).
257. Li, Z., Ding, K. & Ma, G. Eigenvalue knots and their isotopic equivalence in three-state non-Hermitian systems. *Phys. Rev. Res.* **5**, 23038 (2023).
258. Huber, S. D. Topological mechanics. *Nat. Phys.* **12**, 621–623 (2016).
259. Ma, G., Xiao, M. & Chan, C. T. Topological phases in acoustic and mechanical systems. *Nat. Rev. Phys.* **1**, 281–294 (2019).
260. Miniaci, M. & Pal, R. K. Design of topological elastic waveguides. *J. Appl. Phys.* **130**, 141101 (2021).
261. Yves, S., Ni, X. & Alù, A. Topological sound in two dimensions. *Ann. N. Y. Acad. Sci.* **1517**, 63–77 (2022).
262. Fleury, R., Khanikaev, A. B. & Alù, A. Floquet topological insulators for sound. *Nat. Commun.* **7**, 11744 (2016).
263. Gong, Z. et al. Topological phases of non-Hermitian systems. *Phys. Rev. X* **8**, 31079 (2018).
264. Kawabata, K., Shiozaki, K., Ueda, M. & Sato, M. Symmetry and topology in non-Hermitian physics. *Phys. Rev. X* **9**, 41015 (2019).
265. Bergholtz, E. J., Budich, J. C. & Kunst, F. K. Exceptional topology of non-Hermitian systems. *Rev. Mod. Phys.* **93**, 15005 (2021).
266. Ding, K., Fang, C. & Ma, G. Non-Hermitian topology and exceptional-point geometries. *Nat. Rev. Phys.* **4**, 745–760 (2022).
267. Kunst, F. K., Edvardsson, E., Budich, J. C. & Bergholtz, E. J. Biorthogonal bulk–boundary correspondence in non-Hermitian systems. *Phys. Rev. Lett.* **121**, 26808 (2018).
268. Wang, M., Ye, L., Christensen, J. & Liu, Z. Valley physics in non-Hermitian artificial acoustic boron nitride. *Phys. Rev. Lett.* **120**, 246601 (2018).
269. Hu, B. et al. Non-Hermitian topological whispering gallery. *Nature* **597**, 655–659 (2021).
270. Rosendo López, M., Zhang, Z., Torrent, D. & Christensen, J. Multiple scattering theory of non-Hermitian sonic second-order topological insulators. *Commun. Phys.* **2**, 132 (2019).
271. Zhang, Z., Rosendo López, M., Cheng, Y., Liu, X. & Christensen, J. Non-Hermitian sonic second-order topological insulator. *Phys. Rev. Lett.* **122**, 195501 (2019).
272. Zhu, W. et al. Simultaneous observation of a topological edge state and exceptional point in an open and non-Hermitian acoustic system. *Phys. Rev. Lett.* **121**, 124501 (2018).
273. Ni, X. et al. PT phase transitions of edge states at PT symmetric interfaces in non-Hermitian topological insulators.*Phys. Rev. B* **98**, 165129 (2018).
274. Gao, H. et al. Observation of topological edge states induced solely by non-Hermiticity in an acoustic crystal. *Phys. Rev. B* **101**, 180303 (2020).
275. Zhang, K. et al. Observation of topological properties of non-Hermitian crystal systems with diversified coupled resonators chains. *J. Appl. Phys.* **130**, 64502 (2021).
276. Gao, H. et al. Non-Hermitian route to higher-order topology in an acoustic crystal. *Nat. Commun.* **12**, 1888 (2021).
277. Okuma, N., Kawabata, K., Shiozaki, K. & Sato, M. Topological origin of non-Hermitian skin effects. *Phys. Rev. Lett.* **124**, 86801 (2020).
278. Zhang, K., Yang, Z. & Fang, C. Correspondence between winding numbers and skin modes in non-Hermitian systems. *Phys. Rev. Lett.* **125**, 126402 (2020).
279. Yao, S. & Wang, Z. Edge states and topological invariants of non-Hermitian systems. *Phys. Rev. Lett.* **121**, 86803 (2018).
280. Yokomizo, K. & Murakami, S. Non-Bloch band theory of non-Hermitian systems. *Phys. Rev. Lett.* **123**, 66404 (2019).
281. Lin, R., Tai, T., Li, L. & Lee, C. H. Topological non-Hermitian skin effect. *Front. Phys.* **18**, 53605 (2023).
282. Zhang, L. et al. Acoustic non-Hermitian skin effect from twisted winding topology. *Nat. Commun.* **12**, 6297 (2021).
283. Gu, Z. et al. Transient non-Hermitian skin effect. *Nat. Commun.* **13**, 7668 (2022).
284. Zhang, X., Tian, Y., Jiang, J.-H., Lu, M.-H. & Chen, Y.-F. Observation of higher-order non-Hermitian skin effect. *Nat. Commun.* **12**, 5377 (2021).
285. Rosa, M. I. N. & Ruzzene, M. Dynamics and topology of non-Hermitian elastic lattices with non-local feedback control interactions. *N. J. Phys.* **22**, 53004 (2020).
286. Scheibner, C., Irvine, W. T. M. & Vitelli, V. Non-Hermitian band topology and skin modes in active elastic media. *Phys. Rev. Lett.* **125**, 118001 (2020).
287. Wang, W., Wang, X. & Ma, G. Non-Hermitian morphing of topological modes. *Nature* **608**, 50–55 (2022).
288. Gao, P., Willatzen, M. & Christensen, J. Anomalous topological edge states in non-Hermitian piezophononic media. *Phys. Rev. Lett.* **125**, 206402 (2020).

Acknowledgements

L.H. and A.E.M. were supported by the Australian Research Council Discovery Project (DP200101353) and the UNSW Scientia Fellowship programme. S.H. and Y.L. were supported by the Shanghai Science and Technology Committee (grant nos. 21JC1405600). C.S. was supported by the US National Science Foundation under grant no. CMMI-2137749. S.Y., X.N., S.K. and A.A. were supported by the Air Force Office of Scientific Research and Simons Foundation. A.S.P and A.F.S acknowledge the state assignment of Kirensky Institute of Physics. Y.K.C. and D.A.P. were supported by the Australian Research Council Discovery Project (grant no. DP200101708).

Author contributions

L.H., S.H., C.S., S.Y. and A.S.P. provided initial drafts of portions of the manuscript. All authors subsequently integrated, reviewed and revised the full manuscript.

Competing interests

The authors declare no competing interests.

Additional information

Supplementary information The online version contains supplementary material available at https://doi.org/10.1038/s42254-023-00659-z.

Peer review information *Nature Reviews Physics* thanks Nicholas Fang, Ching Hua Lee and Guancong Ma for their contribution to the peer review of this work.